

**EUR 4877 e**

COMMISSION OF THE EUROPEAN COMMUNITIES

**CALCULATIONS ON THE IN-PILE BEHAVIOUR  
OF FISSION GAS IN OXIDE FUELS**  
An Extended Parametric Study

by

C. RONCHI and Hj. MATZKE

1972



Joint Nuclear Research Centre  
Karlsruhe Establishment - Germany  
European Institute for Transuranium Elements

## LEGAL NOTICE

This document was prepared under the sponsorship of the Commission of the European Communities.

Neither the Commission of the European Communities, its contractors nor any person acting on their behalf:

make any warranty or representation, express or implied, with respect to the accuracy, completeness, or usefulness of the information contained in this document, or that the use of any information, apparatus, method or process disclosed in this document may not infringe privately owned rights; or

assume any liability with respect to the use of, or for damages resulting from the use of any information, apparatus, method or process disclosed in this document.

This report is on sale at the addresses listed on cover page 4

at the price of B.Fr. 100,-

**Commission of the  
European Communities**  
**D.G. XIII - C.I.D.**  
29, rue Aldringen  
L u x e m b o u r g

December 1972

This document was reproduced on the basis of the best available copy.

**EUR 4877 e**

**CALCULATIONS ON THE IN-PILE BEHAVIOUR OF FISSION GAS  
IN OXIDE FUELS - An Extended Parametric Study**  
by C. RONCHI and Hj. MATZKE

Commission of the European Communities  
Joint Nuclear Research Centre - Karlsruhe Establishment (Germany)  
European Institute for Transuranium Elements  
Luxembourg, December 1972 - 78 Pages - 64 Figures - B.Fr. 100.—

Model calculations on fission gas behaviour and fuel swelling during reactor operation are presented. In its present form, the model allows to quantitatively calculate the contribution of single gas atom diffusion to the overall fission gas behaviour, a contribution which previously was frequently neglected. Thus the model includes gas atom diffusion, precipitation into a constant number of bubbles of variable size, multiple fission induced re-resolution of gas atoms from bubbles and precipitation at grain boundaries which are regarded to be deep sinks. Numerical solutions have been obtained for

---

**EUR 4877 e**

**CALCULATIONS ON THE IN-PILE BEHAVIOUR OF FISSION GAS  
IN OXIDE FUELS - An Extended Parametric Study**  
by C. RONCHI and Hj. MATZKE

Commission of the European Communities  
Joint Nuclear Research Centre - Karlsruhe Establishment (Germany)  
European Institute for Transuranium Elements  
Luxembourg, December 1972 - 78 Pages - 64 Figures - B.Fr. 100.—

Model calculations on fission gas behaviour and fuel swelling during reactor operation are presented. In its present form, the model allows to quantitatively calculate the contribution of single gas atom diffusion to the overall fission gas behaviour, a contribution which previously was frequently neglected. Thus the model includes gas atom diffusion, precipitation into a constant number of bubbles of variable size, multiple fission induced re-resolution of gas atoms from bubbles and precipitation at grain boundaries which are regarded to be deep sinks. Numerical solutions have been obtained for

---

**EUR 4877 e**

**CALCULATIONS ON THE IN-PILE BEHAVIOUR OF FISSION GAS  
IN OXIDE FUELS - An Extended Parametric Study**  
by C. RONCHI and Hj. MATZKE

Commission of the European Communities  
Joint Nuclear Research Centre - Karlsruhe Establishment (Germany)  
European Institute for Transuranium Elements  
Luxembourg, December 1972 - 78 Pages - 64 Figures - B.Fr. 100.—

Model calculations on fission gas behaviour and fuel swelling during reactor operation are presented. In its present form, the model allows to quantitatively calculate the contribution of single gas atom diffusion to the overall fission gas behaviour, a contribution which previously was frequently neglected. Thus the model includes gas atom diffusion, precipitation into a constant number of bubbles of variable size, multiple fission induced re-resolution of gas atoms from bubbles and precipitation at grain boundaries which are regarded to be deep sinks. Numerical solutions have been obtained for

many different sets of parameters for typical irradiation conditions in both fast and thermal reactors. Typical results are given in the text, and the broad parametric study is contained in Appendices. The equated quantities are the concentrations of gas in dynamical solution, in intragranular bubbles and at grain boundaries, as well as the local swelling rate.

As a typical example, some calculations for a fast flux irradiation experiment (DS irradiation) with mixed (U, Pu) oxides are given which show that experimental swelling curves can be reasonably well predicted with acceptable parameters. Conversely, the comparison of calculations and experimental results can serve to better determine such important parameters as effective in-pile diffusion coefficients. In addition, the relative importance of gas bubble mobility and sweeping phenomena etc. can be evaluated in this way.

---

many different sets of parameters for typical irradiation conditions in both fast and thermal reactors. Typical results are given in the text, and the broad parametric study is contained in Appendices. The equated quantities are the concentrations of gas in dynamical solution, in intragranular bubbles and at grain boundaries, as well as the local swelling rate.

As a typical example, some calculations for a fast flux irradiation experiment (DS irradiation) with mixed (U, Pu) oxides are given which show that experimental swelling curves can be reasonably well predicted with acceptable parameters. Conversely, the comparison of calculations and experimental results can serve to better determine such important parameters as effective in-pile diffusion coefficients. In addition, the relative importance of gas bubble mobility and sweeping phenomena etc. can be evaluated in this way.

---

many different sets of parameters for typical irradiation conditions in both fast and thermal reactors. Typical results are given in the text, and the broad parametric study is contained in Appendices. The equated quantities are the concentrations of gas in dynamical solution, in intragranular bubbles and at grain boundaries, as well as the local swelling rate.

As a typical example, some calculations for a fast flux irradiation experiment (DS irradiation) with mixed (U, Pu) oxides are given which show that experimental swelling curves can be reasonably well predicted with acceptable parameters. Conversely, the comparison of calculations and experimental results can serve to better determine such important parameters as effective in-pile diffusion coefficients. In addition, the relative importance of gas bubble mobility and sweeping phenomena etc. can be evaluated in this way.

**EUR 4877 e**

COMMISSION OF THE EUROPEAN COMMUNITIES

CALCULATIONS ON THE IN-PILE BEHAVIOUR  
OF FISSION GAS IN OXIDE FUELS  
An Extended Parametric Study

by

C. RONCHI and Hj. MATZKE

1972



Joint Nuclear Research Centre  
Karlsruhe Establishment - Germany  
European Institute for Transuranium Elements

## ABSTRACT

Model calculations on fission gas behaviour and fuel swelling during reactor operation are presented. In its present form, the model allows to quantitatively calculate the contribution of single gas atom diffusion to the overall fission gas behaviour, a contribution which previously was frequently neglected. Thus the model includes gas atom diffusion, precipitation into a constant number of bubbles of variable size, multiple fission induced re-solution of gas atoms from bubbles and precipitation at grain boundaries which are regarded to be deep sinks. Numerical solutions have been obtained for many different sets of parameters for typical irradiation conditions in both fast and thermal reactors. Typical results are given in the text, and the broad parametric study is contained in Appendices. The equated quantities are the concentrations of gas in dynamical solution, in intragranular bubbles and at grain boundaries, as well as the local swelling rate.

As a typical example, some calculations for a fast flux irradiation experiment (DS irradiation) with mixed (U, Pu) oxides are given which show that experimental swelling curves can be reasonably well predicted with acceptable parameters. Conversely, the comparison of calculations and experimental results can serve to better determine such important parameters as effective in-pile diffusion coefficients. In addition, the relative importance of gas bubble mobility and sweeping phenomena etc. can be evaluated in this way.

## KEYWORDS

RADIATION EFFECTS	SWELLINGS
FUELS	DIFFUSION
URANIUM OXIDES	PRECIPITATION
PLUTONIUM OXIDES	BUBBLES
FISSION PRODUCTS	MATHEMATICAL MODELS
GASES	NUMERICAL SOLUTION
ATOMS	

Contents

	page
1. Introduction	5
2. The mathematical model	6
2.1. Precipitation of gas in the absence of irradiation	6
2.2. Behavior of the gas under reactor conditions	9
a) The resolution of gas	
b) Precipitation of gas at grain boundaries	
2.3. Quantitative description of the behavior of the gas	11
2.4. Limits of Application	12
3. Application of the model to the fast irradiation experiments DS1 and DS2	13
3.1. Time and temperature dependence of c (gas in atomic (dynamical) solution)	15
3.2. Time and temperature dependence of g (gas precipitated at grain boundaries)	17
3.3. Time and temperature dependence of b (gas precipitated in intragranular bubbles)	18
3.4. Comparison with post-irradiation examination	21
4. Some remarks on the choice of the parameters	23
5. Conclusions and Summary	24
References	25
List of Symbols	27
Appendices	
I : Derivation of the precipitation laws	28
II : On the choice of the resolution parameter	30
III : On the choice of the gas diffusion coefficients	32
IV : Model simplified with the assumption that all gas atoms are trapped in intra-granular bubbles before being released	36
Parametric study	
V : Thermal reactor conditions	41
VI : Calculations for fast flux irradiation and different typical fuel temperatures	45
VII : Parametric study ( $D, n, \eta$ ) for fuel temperatures of	52

1000°C, 1500°C and 2500°C

- VIII : Variation of the resolution probability at 66  
a fuel temperature of 1200°C.
- IX : Variation of the gas diffusion coefficient, D, 70  
and the grain size, a, at a fuel temperature of 2000°C

## 1. Introduction

The behavior of fission gases in ceramic fuels has been studied experimentally and calculations on gas behavior in fuel elements have been performed since about 1957 (e.g.1,2), the emphasis, however, of these studies has changed several times. In the first years, gas release alone was thought to be of importance, mainly because of the fear that excessive fission gas pressure might cause fuel failure. Later, more sophisticated engineering techniques provided possibilities of accomodating released gases, and fuel swelling was considered to be of more interest, especially after the first irradiations in a fast flux and high burn-ups from thermal reactor irradiations were available. At about the same time, trapping of gas in form of interactions of fission gas atoms with either pre-existing or radiation-induced defects (3) and the formation of gas-filled bubbles (e.g.4) were noted to be of importance. The basic physical processes of trapping and of bubble nucleation, growth, and mobility were studied in some detail (e.g. 5-8), and a number of theories and model calculations on the effects of bubbles (e.g. 9-10) were performed. Subsequently, the observation of the disappearance of pre-formed bubbles was confirmed during irradiations at low temperature, (e.g. 11-13), i.e. the existence of a fission induced resolution of precipitated gas was proven. The older theories did not allow for this effect, some of the more recent ones did (e.g. 13, 14)<sup>+</sup>, but quantitative calculations on its importance for the migration of gas to grain boundaries and hence on the contribution of single gas atom diffusion to the overall release seem to miss so far. The present paper intends to close this gap.

---

<sup>+</sup> The references given so far are typical ones but do by no means fully represent the extensive literature. A more comprehensive literature survey on fission gas release and bubble mobility studies in UO<sub>2</sub> has recently been presented in ref.(15). Recent theoretical treatments are comprised in the Proceedings of the Symposium on Theoretical Models for Predicting In-Reactor Performance of Fuel and Cladding Material (16).

## 2. The mathematical model

In this section we want to develop the mathematics to calculate as function of temperature, burn-up, fission rate, and power history: i) the concentration,  $c$ , of dissolved gas; ii) the concentration,  $b$ , of gas precipitated into intragranular bubbles, and iii) the concentration,  $g$ , of gas that precipitated at grain boundaries and eventually is released to the plenum. Then, if  $\beta$  is the production rate of gas and, hence,  $\beta t$  the total <sup>amount</sup> of gas produced, the relation holds

$$\beta t = c + b + g \quad (1)$$

thus yielding a complete balance of the fission gases.

### 2.1 Precipitation of gas in the absence of irradiation

The first step for resolving the problem is to correlate the distribution of gas-filled bubbles with the concentration of gas atoms in solution. To this end, we introduce the simplifying assumption of a homogeneous distribution of bubble nuclei, and hence of the existence of a certain constant volume,  $\Delta V$ , surrounding each bubble nucleus, as indicated in Fig. 1a.

If  $c$  is the concentration of gas in solution and using the nomenclature as indicated in Fig. 1b, we have

- within the volume element  $\Delta V$ : 
$$\frac{\partial c}{\partial t} = - D \nabla^2 c \quad (2)$$

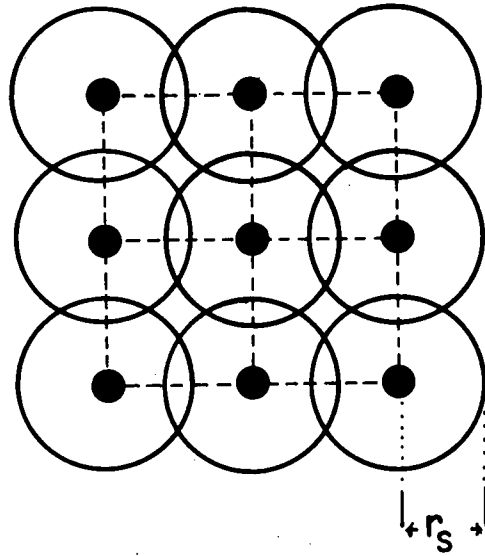
- at the surface of the bubble ( $r = r_0$ ):  $c(r_0) = c_1 \quad (2a)$

Since the boundary conditions for the diffusion equation are quite complicated, we introduce as a further reasonable and simplifying assumption that the net flux of gas atoms through the surfaces of the volume elements,  $\Delta V$ , be negligible, i.e. that

$$\oint_{\vec{n}} \vec{n} \cdot (-D \nabla c) = 0 \quad (2b)$$

If  $n$  is the concentration of bubbles, and assuming that the  $\Delta V$  influenced by any individual bubble are spherical with radius,  $\rho$ , we get

$$\frac{1}{n} = \frac{4}{3} \pi \rho^3 \quad (3)$$



● bubble with radius,  $r_0$

Fig. 1a : Schematic representation of the assumption on bubble distribution and size and shape of the precipitation volumes,  $\Delta V$ .

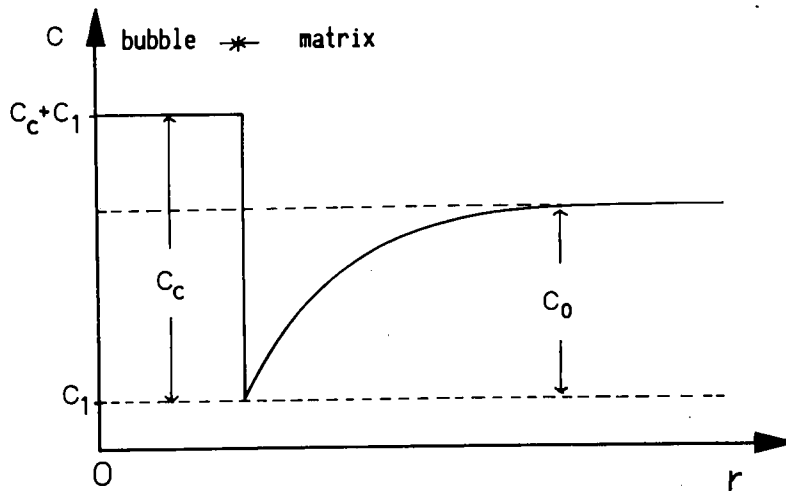


Fig. 1b : Schematic representation of the concentration of gas in solution around a bubble in a matrix containing a supersaturation of fission gas.

The boundary condition (2b) has for this case the simple form

$$\left(\frac{\partial c}{\partial r}\right)_{r=\varrho} = 0$$

Equation (2) with the boundary conditions (2a) and (2b) is well known. A procedure for its solution has been given by e.g. Ham (17), (see also Appendix I).

As the final result, we obtain :

near to the bubble

$$c = c_0 \exp(-t/\tau_0) (1-r_0/r) \quad \text{for } r \approx r_0 \quad (4a)$$

and, far away from the bubble

$$c = c_0 \exp(-t/\tau_0) \quad \text{for } r \gg r_0 \quad (4b)$$

where  $\tau_0 = \varrho^3/3r_0 D$ .

If we assume that  $r_0 \ll \varrho$ , the kinetics of precipitation of most of the gas are described by Equ. (4b), hence by an equation which is independent of  $r$ . By differentiation we get

$$dc = - \frac{c}{\tau_0} dt. \quad (4b')$$

This implies a relation between bubble radius,  $r_0$ , and bubble concentration,  $n$ , such that

$$\begin{aligned} n < 10^{15} \text{ cm}^{-3} & \quad \text{for } r_0 \sim 10 \text{ \AA} \\ n < 10^{14} \text{ cm}^{-3} & \quad \text{for } r_0 \sim 100 \text{ \AA} . \end{aligned}$$

The above assumption ( $r_0 \ll \varrho$ ) is the most restrictive one made so far\*. It restricts the calculations to those cases where the bubbles are small compared to the bubble spacing.

Such conditions are indeed frequently observed in post irradiation examinations of oxide fuels (e.g. 18), though there exist other investigations (e.g. 19) which indicate larger bubble concentrations. For such cases, a separate mathematical treatment must be made. Here, we just want to note that very large bubble concentrations which imply bubble spacings of the order of the bubble radii, were only

---

\* If  $r_0$  becomes comparable to  $\varrho$  (i.e. in the cases of either very big bubbles or alternatively very high bubble concentrations), Equ.(4a) will yield an overestimation of  $c$  for small values of time. For  $t \rightarrow \infty$ , however, the differential equation (4b') will represent a satisfactory approximation even in these extreme cases.

occasionally observed in the replica electron microscope investigation of the fast irradiation DS , and in particular zones of the fuel only (see below). In these zones, the accumulation of bubbles could always be explained by specific mechanisms (e.g. sweeping by moving sub-grain boundaries etc.), and these few zones were not typical of the fuel matrix.

If we thus accept equs. (4), we have the solution for the behaviour of the gas in solution in a solid having a constant initial gas concentration. This behaviour is indicated in Fig. 1b.

## 2.2. Behavior of the gas under reactor conditions.

The conditions in a fuel element under operation are more complicated. To approach these conditions, we have to take into account that

- a) gas is produced continuously with a given rate,  $\beta$  (in the following assumed to be constant)
- b) fission events cause a certain resolution of the gas due to knock-on processes of gas atoms with either fission fragments or atoms of the collision cascades produced by the fission fragments
- c) a certain amount of gas precipitates at grain boundaries where it may behave differently from gas in an intragranular bubble.

### a) The resolution of gas

For the present calculations, we accept the resolution model of Nelson (20). If a bubble of radius,  $r_0$ , is bombarded with fission products, the resolution rate,  $\Gamma$ , is given by

$$\Gamma = \frac{4\pi r_0^2 d\eta}{\beta} \quad (5)$$

where  $\beta$  is the co-volume (Van der Waals constant) of the gas,  $d$  is the thickness of the shell within a bubble from which a gas atom may be ejected with a certain probability,  $\eta$ . Since  $\eta$  decreases strongly with increasing  $d$ , we assume for the further calculations that only atoms from a shell of thickness,  $d$ , of  $10 \text{ \AA}$  can be finally resolved. The value of  $\eta$  can either be calculated on basis of a certain physical model (see below); alternatively it can be measured directly by observing the fission dose necessary to destroy a pre-formed bubble population; or else the parameter  $d \cdot \eta$  can simply be

regarded as a phenomenological quantity. For the present purpose it will suffice to note that the most probable values for  $\eta$  fall into the range  $10^{-4}$  to  $10^{-6}$   $\text{sec}^{-1}$  and depend on the fission rate,  $\dot{S}$  (see Section 4 and Appendix II).

If we further assume that the growth of the bubbles does not create strains around their surfaces, the concentration (in moles) of gas contained in a bubble is given by

$$m = \frac{8\pi\gamma r_0^2}{3RT}$$

where  $\gamma$  is the surface tension of the solid. With a concentration,  $n$ , of bubbles and a homogeneous growth, we get

$$\frac{Bt - c^*}{n} = \frac{8\pi\gamma r_0^2}{3RT}$$

where  $B$  again is the production rate of the fission gas, and  $c^*$  the concentration of gas that is not precipitated in bubbles. If we introduce this relation in Equ. (5), we get for the resolution rate

$$\Gamma = (Bt - c^*) \frac{3}{2} \frac{RTd\eta}{b\gamma} \quad (5a)$$

#### b) Precipitation of Gas at Grain Boundaries

The flux of gas towards grain boundaries can be calculated by using the well known (e.g. 1) relation

$$g = c \left[ 1 - \sum_{n=1}^{\infty} \frac{6}{\pi^2 n^2} \exp(-n^2 \pi^2 Dt/a^2) \right]$$

where  $g$  = concentration of fission gas in grain boundaries,  $a$  = radius of the grains and  $D$  = effective diffusion coefficient for the migration of fission gas atoms. Therefore

$$\frac{dg}{dt} = \text{Pos}\left(\frac{dc}{dt}\right) \left[ 1 - \sum_{n=1}^{\infty} \frac{6}{\pi^2 n^2} \exp(-n^2 \pi^2 Dt/a^2) + \frac{6cD}{a^2} \sum_{n=1}^{\infty} \exp(-n^2 \pi^2 Dt/a^2) \right] \quad (6)$$

where  $\text{Pos}(f(x))$  is an operator defined by  $\text{Pos}(f(x)) = \frac{1}{2} [f(x) + |f(x)|]$ .

This treatment assumes that the gas is deeply trapped at or released soon from the grain boundary. No allowance is made, at this stage, for other mechanisms than atomic diffusion for the transport of the gas to the boundary (see Sections 1 and 24).

### 2.3. Quantitative description of the behaviour of the gas

We may now quantitatively describe the behaviour of the gas subject to the above mentioned conditions :

- continuous creation by fission
- precipitation in bubbles
- resolution by fission events
- migration of resolved gas to grain boundaries
- trapping at and/or release from grain boundaries.

The relevant differential equation can be written in the form

$$dc_{\text{solut.}} = dc_{\text{creat.}} + dc_{\text{resolut.}} - dc_{\text{precip.}} - dc_{\text{g.b.}}$$

where the differentials at the right hand side are obtained from equs. (4 b), (5), and (6). After some lengthy but straight forward calculations, we obtain

$$\frac{dc}{dt} = \beta - \frac{Kc}{\sqrt{\beta}} (\beta t - c - g)^{1/2} + C (\beta t - c - g) - \frac{dg}{dt}$$

$$\frac{dg}{dt} = P_{\text{os}} \left( \frac{dc}{dt} \right) \left[ 1 - \sum_{n=1}^{\infty} \frac{6}{\pi^2 n^2} \exp(-n^2 \pi^2 Dt/a^2) + \frac{6cD}{a^2} \sum_{n=1}^{\infty} \exp(-n^2 \pi^2 Dt/a^2) \right] \quad (7)$$

with

$$K = D \frac{(6\pi n BRT)^{1/2}}{\gamma} \quad C_0 = \frac{3}{2} \frac{RTd\eta}{b\gamma}$$

Equs. (7) are a system of linear differential equations the solution of which determines the integral functions  $c(t)$  and  $g(t)$ , i.e. the concentration of fission gas in dynamical solution and trapped at grain boundaries. Two additional quantities of interest, that can easily be obtained in the course of the computation, are the concentration,  $b$ , of gas precipitated in intragranular bubbles, and the local swelling due to the bubbles,  $(\Delta V/V)_{\text{local}}$ . Computation has to be done numerically with the aid of a computer.

#### 2.4. Limits of Application

After having derived the mathematics, we want to discuss the applicability of the above equations. The restrictions imposed by the mathematical approximation while solving Equ. (2) have already been mentioned. The solution (4b) represents indeed a fairly simple situation where the gas concentration is independent of the space coordinates. Its validity falls if  $\varphi$  becomes small enough. However, even for such more complicated cases, it is always possible to obtain the correct solution by using a more suitable space and time dependent precipitation rule<sup>+</sup>. Obviously, in such a case, the coordinate  $r$  would also appear in Equ. (7) and an integration over  $r$  in  $\Delta V$  would become necessary for getting an average of  $c(t)$ . As discussed in Section 2.1 and below, however, existing experimental evidence is compatible with the simple approach used here which, beyond that, is adequate to treat the problem of this paper.

Another point that should be discussed is the boundary condition (2b). Actually, if a net flux of gas atoms flows towards the grain boundary,  $\phi$  will be  $< 0$  on the side of  $\Delta V$  which is nearer to the grain boundary, and it will be  $> 0$  on the opposite side. To obtain Equ. (7), this flux was assumed to be negligible and thus to not affect the gas concentration within each  $\Delta V$ . This assumption is obviously reasonable only if  $\Delta V$  is small compared to the grain size which is the case for most experimental conditions. Yet, one has to realize that the presented model loses its validity not only for very high, but also for very low bubble concentrations.

The second type of restrictions originates from the assumed physical features. Some important phenomena were willingly disregarded in the present treatment :

- a) the dependence of the nucleation density for bubbles on the irradiation conditions
- b) the mobility of bubbles at high temperatures
- c) the sweeping of bubbles due to moving dislocations, dislocation networks, and grain boundaries
- d) the resolution of gas precipitated at grain boundaries

<sup>+</sup>Such a more elaborate rule would lead to a slightly smaller value of  $b$  and would not affect its asymptotic behavior shown in Section 3.3

- e) the effect of the thermal gradient (thermodiffusion)

- f) the effect of solid fission products

A quantitative treatment of the second and third of these phenomena is certainly not necessary below temperatures at which self-diffusion processes are sufficiently slow ( $D_{sd} \leq 10^{-12} \text{ cm}^2 \text{ sec}^{-1}$ , corresponding to a bubble mobility of about 1  $\mu\text{m}$  per month in a typical oxide fuel and for a volume diffusion mechanism for bubble mobility).

Thus, the model should fully represent the behaviour of fission gases in fuel zones which are below certain temperatures. These are roughly  $1800^\circ\text{C}$  for oxides (21). Even for higher temperatures, the model yields a fair prediction of the contribution of atomic scale diffusion to the overall behavior of the gas. At these temperatures, bubble mobilities and sweeping phenomena get more important. A typical bubble velocity near the center of the fuel will be about 300  $\mu\text{m}/\text{month}$  and will thus be comparable to the velocity of the migration of single gas atoms. Even in this case, the competing processes of resolution and precipitation establish an equilibrium between free gas atoms and gas trapped in bubbles that can be adequately described by the presented model provided realistic assumptions on the bubble nucleation densities are introduced. It will be shown below that the contribution of single gas atoms alone satisfactorily explains experimental results on the general behavior of fission gases in oxide fuels thus serving as indication that the bubble mobility processes are not necessarily the factor determining the reactor behavior.

Fig. 2 recalls once more the general assumptions made while establishing the model.

### 3. Application of the model to the fast irradiation experiments

#### DS1 and DS2.

In the following, first results of the calculations will be presented.

To this end, curves are shown which give the time (or burn-up)

dependence of the four most important quantities

c, concentration of gas in dynamical solution

g, concentration of gas at grain boundaries

b, concentration of gas in intragranular bubbles

( $\Delta V/V$ )<sub>local</sub>, the local swelling due to intragranular bubbles.

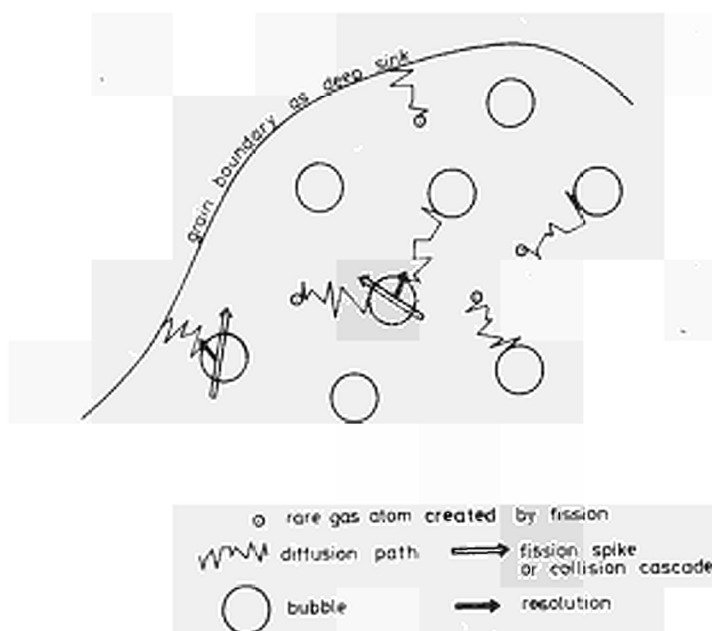


Fig. 2 : Sketch illustrating the assumptions on transport of fission gas atoms towards grain boundaries.

Table I

Parameters for "normal conditions"

Temperature ( $^{\circ}\text{C}$ )	1000	1200	1500	2000	2500
D ( $\text{cm}^2 \text{sec}^{-1}$ )	$1.5 \times 10^{-16}$	$2 \times 10^{-14}$	$5 \times 10^{-12}$	$1 \times 10^{-9}$	$3 \times 10^{-8}$
a ( $\mu\text{m}$ )	10	10	20	100	100

The micro-structure (grain size, a) and the irradiation condition were taken from the fast irradiation experiment DS1 and its post-irradiation examination (18) :

$$\begin{aligned} \beta &= 2.9 \times 10^{-11} \text{ moles cm}^{-3} \text{sec}^{-1} \\ n &= 10^{14} \text{ cm}^{-3} \end{aligned}$$

The resolution probability (see Section 4 ) was chosen as

$$\eta = 1.9 \times 10^{-5} \text{ sec}^{-1}$$

Furthermore:  $\gamma = 10^3 \text{ erg cm}^{-2}$

For these calculations, a set of "normal" parameters was selected (see table I). As characteristic temperatures, 1000, 1200, 1500, 2000, and 2500°C were chosen, and in addition the effect of radiation enhanced diffusion at low temperatures was calculated.

The production rate,  $\beta$ , and the grain sizes,  $a$ , as well as the bubble density,  $n$ , were chosen as empirical parameters from the fast irradiation experiment DS1 (see ref. (18) for details).

In brief, the DS experiment is a fast flux irradiation of coprecipitated mixed oxide (20 % Pu, U fully enriched) with an original grain size of about 10  $\mu\text{m}$  and varying ratios of O/M of 200, 1.95 or 1.935. The pellet density was high with 96 %, the smear density was 90 %, with a pellet diameter of 5.38 mm. The fuel pins were irradiated with a max. linear power of 565 W/cm at a maximum cladding temperature of 660°C. Following irradiation, both conventional ceramography and an extensive replica electron microscopy study (see ref. (18)) were performed. The grain sizes,  $a$ , were obtained from ceramographic pictures (see Table I); the bubble density was observed to be fairly constant over the pin radius and to fall into the range  $5.10^{13} \text{ cm}^{-3} \leq n \leq 5.10^{14} \text{ cm}^{-3}$ , with a size distribution of the bubbles centered around a maximum of about 300 Å (range 100 to 500 Å). No obvious evidence for bubble mobility was observed. Sweeping phenomena did occur, but were not typical for big areas of the fuel.

The remaining parameters are the resolution rate,  $\eta$ , and the effective gas diffusion coefficient,  $D$ . Both were selected on basis of the arguments of Section 4. In addition, the parameters of  $D$ ,  $a$ ,  $n$ , and  $\eta$  were varied in the course of a broad parametric study. A more complete review of all the computations is presented in the Appendices. In the following some representative results will serve to explain the basic features of the model.

### 3.1. Time and temperature dependence of $c$ (gas in atomic (dynamical) solution).

Fig. 3 shows the variation of the concentration of gas in solution,  $c$ , with irradiation time, for the conditions of Table I and for different temperatures. At the edge of the fuel, at temperatures below 1000°C, most of the gas stays in solution for normal irradiation times (e.g. 75 % of the total created fission gas at  $t = 1$  year and  $T = 1000^\circ\text{C}$ ). For higher temperatures, the percentage of the gas in solution is much smaller, and can be summarized as follows (for

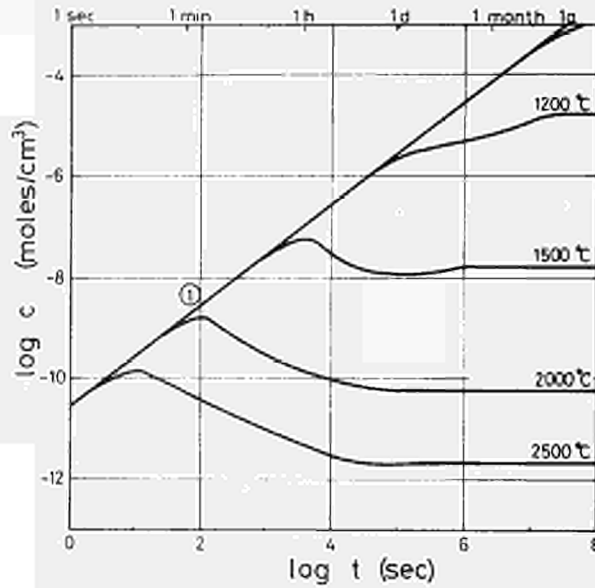


Fig. 3 : Fission gas concentration,  $c$ , in dynamical solution for the conditions of Table I and for different temperatures. Line I represents the production of the rare gas by fission.

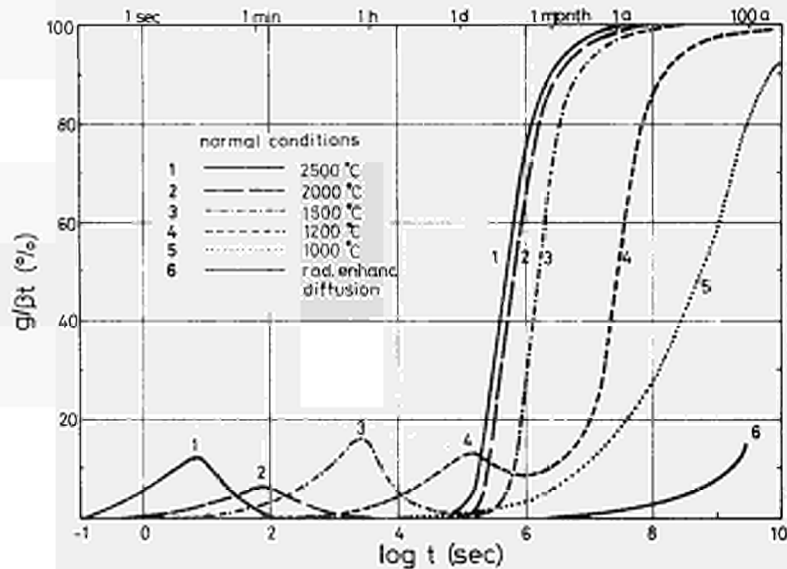


Fig. 4 : Percentage of fission gas precipitated at grain boundaries,  $g/Bt$ , for different temperatures and the conditions of Table I.

the values of D, n, etc. of Table I):

temperature (°C)	irradiation time			
	1 min	1h	1d	1 month
1200	~99	98	80	9
1500	98	54	~0.1	~0
2000	85	~0.1	~0	~0
2500	2	~0.1	~0	~0

A variation of the parameters D, n,  $\eta$ , and a was performed.

The most drastic effect was observed while varying D. For the slowest kinetics possible (lower limit for the effective rare gas diffusion coefficient, D, see Section 4), upper limits for c were obtained. Typical values are 97 % at t = 1 year and T = 1000°C, or 2 % at t = 1 h and T = 2500°C, etc.

In all cases, saturation levels were achieved at high enough values of time. This is typical for the physical assumptions of the presented model, i.e. a fraction of the gas atoms is enabled to escape to the grain boundaries without ever being temporarily trapped in a bubble. In a similar and physically less satisfactory model where all gas atoms are assumed to be trapped in bubbles before they, following resolution, are able to diffuse towards grain boundaries, c reaches a minimum and increases with increasing time (actually with  $\sqrt{t}$ , see Fig. 1 in ref.(22)). At the same time, the quantity g gets smaller (see below and Appendix III).

### 3.2 Time and temperature dependence of g (gas precipitated at grain boundaries)

Fig. 4 shows the percentage of fission gas precipitated at grain boundaries for radiation enhanced diffusion and 5 temperatures for "normal conditions" (Table I). For high temperatures, an essential part of the gas reaches grain boundaries in relatively short irradiation times. This gas can probably be considered to essentially represent the amount of gas released to the plenum, since interlinkage of intergranular bubbles and cracking along grain boundaries during power changes will cause the release of most of this gas, especially in the hot part of the fuel.

The effect of varying the main parameters  $n$ ,  $\eta$ , and  $D$  is shown in Fig. 5 for a fuel temperature of  $1500^{\circ}\text{C}$ . Curve 1 is taken from Fig. 4 and represents the "normal conditions" of Table I. The effect of varying the bubble density ( $n \cdot 100$  stands for a bubble density increased by a factor of 100) is seen to be small. A decrease of a factor of 10 in the resolution probability,  $\eta$ , shifts the curve by a factor of about 5 towards higher values of time. Taking the lowest reasonable limit for  $D$  (see Section 4) has a similar effect.

The maxima in Figs. 4 and 5 at small values of the irradiation time correspond to the free diffusion of gas in the virtually virgin undamaged fuel. As soon as bubble formation sets in (see Section 3.3),  $g$  remains practically constant whereas  $\beta t$  increases thus causing  $g/\beta t$  to decrease again. These maxima are relatively unimportant in practice since the total gas concentration  $\beta t$ , is still small at these small values of  $t$ . Appreciable amounts of gas reach the boundaries only at irradiation times in excess of  $t = 10^5$  sec corresponding to the onset of the steep part of the curves. These parts of the curves are due to gas atoms that had undergone multiple precipitation into and resolution from bubbles.

### 3.3 Time and temperature dependence of $b$ (gas precipitated in intragranular bubbles)

Fig. 6 shows the percentage of gas precipitated into intragranular bubbles for radiation enhanced diffusion and 5 temperatures for the conditions of Table I. The rate of precipitation into bubbles depends strongly on the fuel temperature: at e.g.  $1500^{\circ}\text{C}$ , most of the created gas is in bubbles after <sup>an</sup>irradiation time of only 1 day whereas one month is needed before bubbles form at a fuel temperature of  $1000^{\circ}\text{C}$ . At this temperature,  $b/\beta t$  never increases to 100 %.

At longer irradiation,  $b$  reaches a saturation value because of the resolution effect. Since  $\beta t$  continues to increase,  $b/\beta t$  is seen to decrease. It is interesting to note, that the time for this relative decrease is much less dependent on fuel temperature than the precipitation rate. In fact, for  $t \approx 1$  month,  $b/\beta t$  is very little dependent on fuel temperature and varies only between about 20 and 80 %.

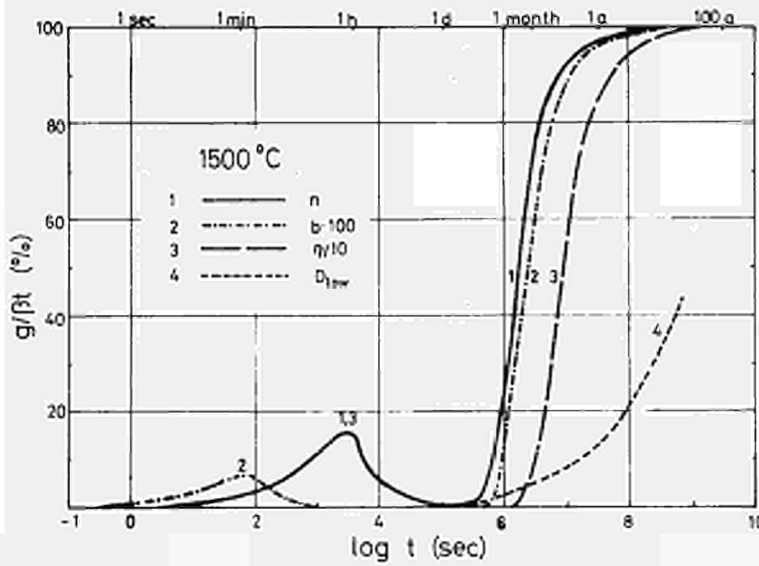


Fig. 5 : Percentage of fission gas precipitated at grain boundaries,  $g/Bt$ , for a fuel temperature of 1500°C and for the conditions of Table I or a variation of either bubble density, gas diffusion coefficient, or resolution probability.

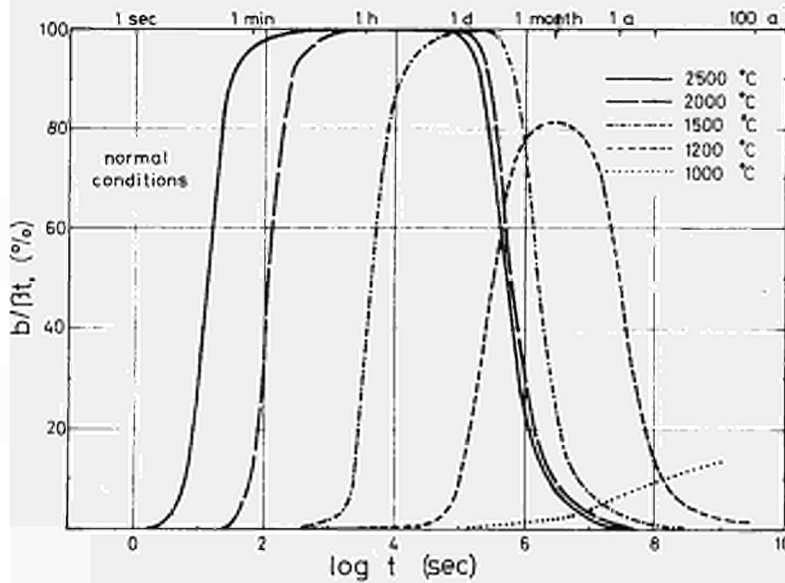


Fig. 6 : Percentage of fission gas precipitated into intragranular bubbles,  $b/Bt$ , for different temperatures and the conditions of Table I.

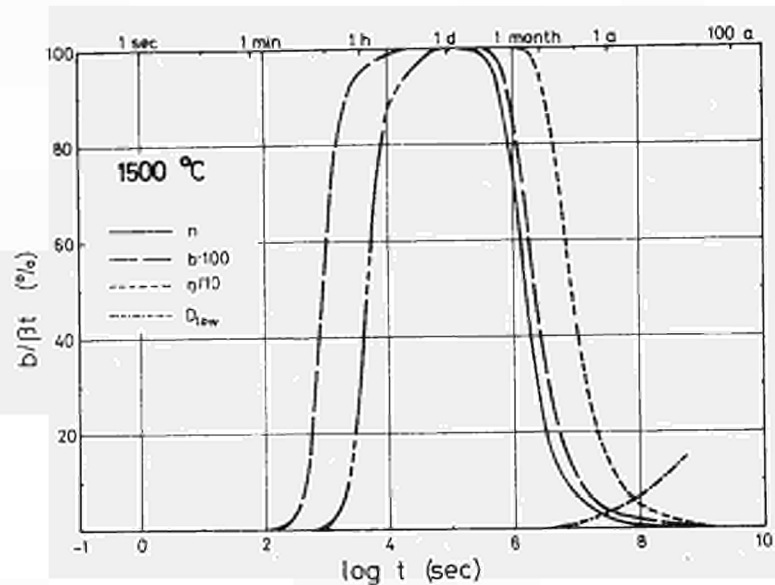


Fig. 7 : Percentage of fission gas precipitated into intragranular bubbles,  $b/Bt$ , for a fuel temperature of  $1500^\circ\text{C}$  and for the conditions of Table I, or a variation of either bubble density, gas diffusion coefficient, or resolution probability.

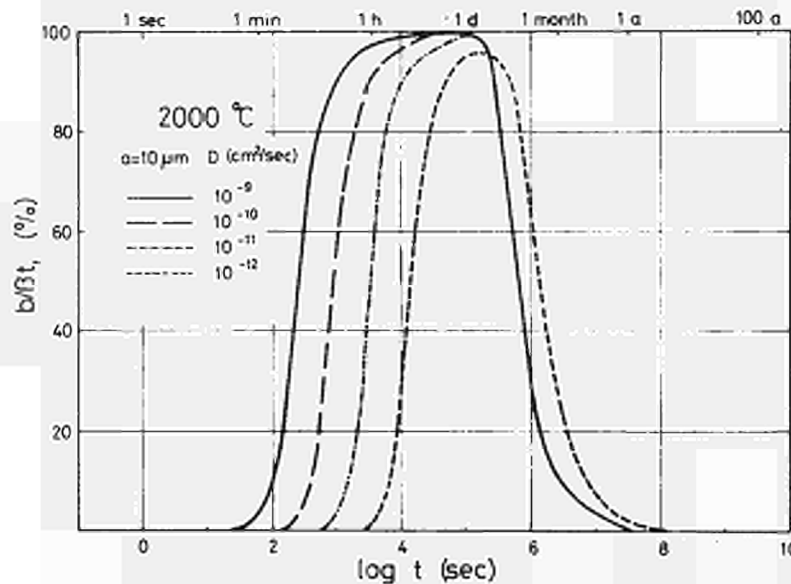


Fig. 8 : Percentage of fission gas precipitated into intragranular bubbles,  $b/Bt$ , for a fuel temperature of  $2000^\circ\text{C}$ , a grain size of  $10\ \mu\text{m}$ , and for 4 values of the gas diffusion coefficient,  $D$ , each varying by a factor of 10.

As in Section 3.2, Fig. 7 shows the effect of varying bubble density (by a factor of 100), resolution rate (by a factor of 10), and the effective gas diffusion coefficient (see Section 4) for a fuel temperature of 1500.

Fig. 8 shows the influence of a systematic variation of the effective gas diffusion coefficient,  $D$ , on the percentage of gas in bubbles at 2000°C. As expected, a decrease in  $D$  leads to a shift towards higher values of time. The range of  $D$ -values considered in Fig. 8 ( $10^{-9}$  to  $10^{-12}$  cm<sup>2</sup> sec<sup>-1</sup>) corresponds to the maximum scatter in literature results (see Section 4).

Finally, Fig. 9 gives a complete balance of the total gas content, again for a fuel temperature of 1500°C and the conditions of Table I. The gas in solution,  $c$ , decreases while bubbles form (increase in  $b$ ). When  $b$  reaches saturation, essential amounts of gas reach grain boundaries (curve for  $g$ , labelled "sinks" in Fig. 9)

#### 3.4 Comparison with post-irradiation examination.

The predictions of the model can successfully be compared with data of the post-irradiation examination of the DS fuel elements. Fig. 10 shows the calculated amount of gas precipitated at grain boundaries as compared to experimental determinations of gas release (dots for about 1 and 7 % burn-up or roughly 1 and 9 months irradiation time (18,23)). The upper curve corresponds to the diffusion coefficients of Table I, the lower one to intermediate values of  $D$  (see Section 4 and Appendix IX). The range of predicted values is seen to closely describe the range of observed release. This agreement indicates that much of the gas is easily transported from the grain boundaries to the plenum.

Fig. 11 finally shows the calculated time dependence of the local swelling for various temperatures. At high temperatures, a saturation in swelling is predicted within a relatively short irradiation time. For conventional irradiation times, the local

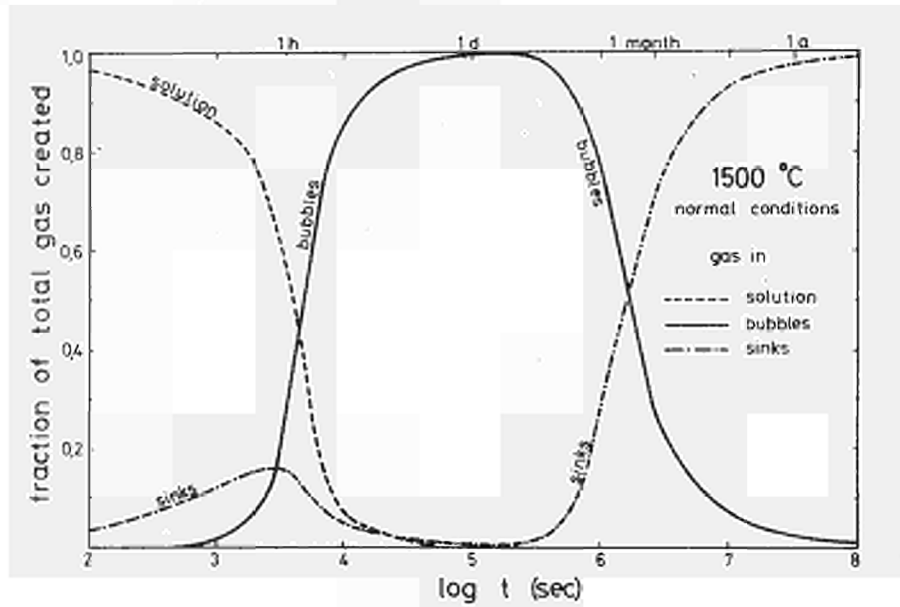


Fig.9 : Balance of total gas, i.e. distribution into gas in solution, in intragranular bubbles, and at grain boundaries for the conditions of Table I and for a fuel temperature of 1500 °C.

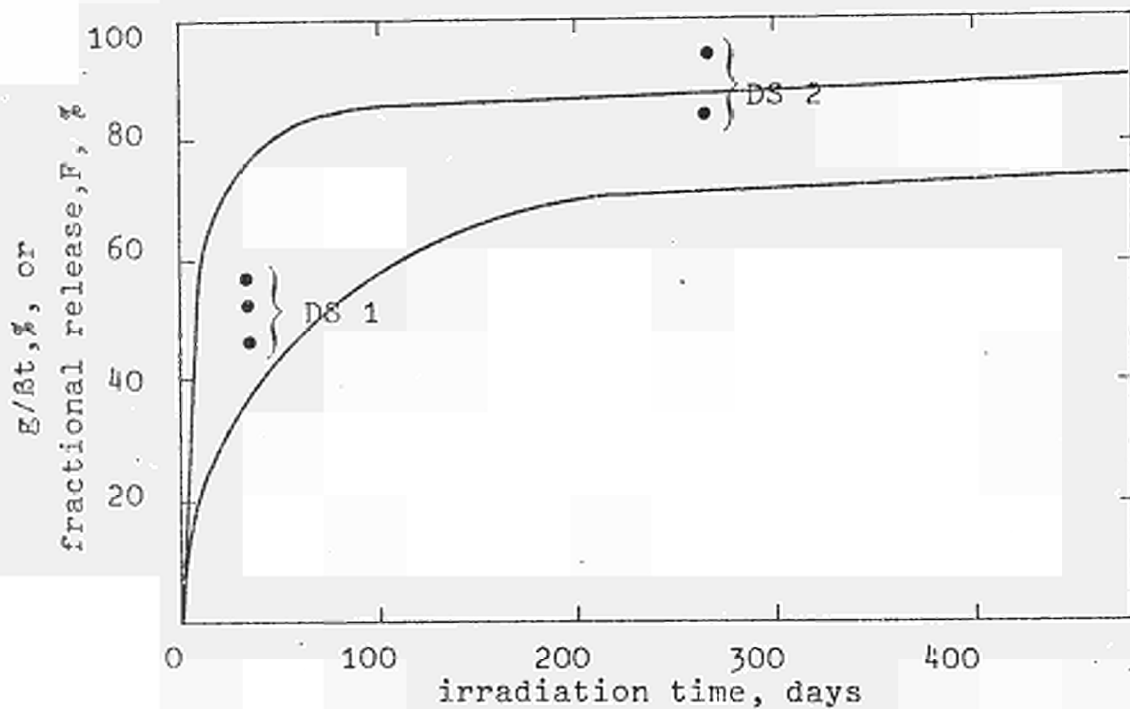


Fig. 10 : Calculated concentration of gas precipitated at grain boundaries for an oxide fuel element of a fast reactor (DS1 and DS2 experiments). Curve a is for high values of the gas diffusion coefficients, curve b for intermediate ones (see Table I and Section 4). The dots represent experimental values of gas release (R.M. Coquerelle, private communication).

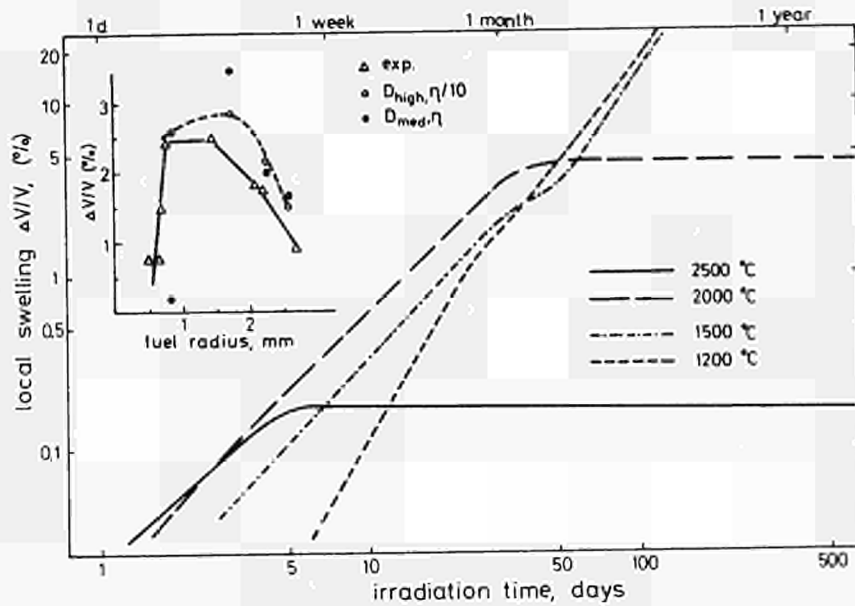


Fig. 11 : Local swelling as function of irradiation time. In the insert, the calculated values are compared with experimental results for the DSL irradiation (see ref. (18)).

swelling has a maximum at intermediate temperatures (between 1500 and 2000°C). In the insert, the calculated swelling for different sets of parameters is compared to experimental results (18). Again, agreement between calculation and experiment is satisfactory given the fact that the calculations were not fitted to the experimental data, but were rather obtained following a selection of what was thought to be the most probable sets of parameters.

#### 4. Some remarks on the choice of the parameters.

The main parameters entering into the model are the grain size,  $a$ , the bubble density,  $n$ , the effective gas diffusion coefficient,  $D$ , and the resolution probability,  $\eta$ . Whereas  $a$  can easily be obtained from the microstructure of the fuel, and a variation of  $n$  does not show any drastic effect (see e.g. Figs. 5 and 7), a proper choice of  $D$  and  $\eta$  is vital for any application of the model. The gas diffusion coefficients were selected from Fig. 9 of ref. (15) where different areas were indicated for the most probable  $D$ -values for either free mobility of gas atoms (so called Stage IIA) or mobility affected by temporary trapping effects (Stage IIB). The  $D$ -values of Table I correspond to the upper boundary of the area for Stage IIA;  $D$ -values referred to

as  $D_{low}$  correspond to the lower boundary of the area for Stage III. The model calculations indicate that the most probable values of  $D$  should be near to those of the boundary between the areas of Stages IIA and B. This would imply that resolution affects trapping of gas atoms as well and that hence many of the very low  $D$ -values obtained for high burn-up oxide during post-irradiation annealing are not representative for in-pile conditions.

The resolution probability  $\eta$  was calculated (see Appendix II) on basis of Nelson's suggestions (20) and considerations of sticking probabilities and thermal desorption. In addition, experimental determinations are available (24,25) yielding a range of about  $3 \times 10^{-5} \text{sec}^{-1}$  to  $3 \times 10^{-4} \text{sec}^{-1}$ . The calculated value is of the order of  $5 \times 10^{-5} \text{sec}^{-1}$  for low temperatures and  $3 \times 10^{-6} \text{sec}^{-1}$  for high temperatures. Therefore,  $\eta$  was varied within this range.

## 5. Conclusions and summary

The present paper presents the equations for calculating the contribution of fission-induced resolution and diffusion of single gas atoms to the overall behavior of the fission gas. In the present stage, the fission gas bubbles were allowed to grow and shrink, but bubble mobility was not included. However, since no empirical relations enter into the model, it can be used in its present form as basis of a more general model which includes bubble mobility and sweeping effects.

The model allows to calculate the concentration of gas in dynamical solution, precipitated into intragranular bubbles and at grain boundaries, as well as the local swelling rate. It is thought to quantitatively describe fission gas behavior at relatively low temperatures (e.g.  $T \leq 1800^\circ\text{C}$  for oxide fuels). In addition, it yields interesting results for all possible fuel temperatures.

Comparison with experimental data of the DS irradiation shows satisfactory agreement. The amount of gas release and of local swelling can be predicted successfully. In addition, the maximum

in swelling at intermediate temperatures observed experimentally follows directly from the model. For high temperatures and irradiations to a few % burn-up, a saturation in swelling is predicted.

This agreement between calculations and post-irradiation examination implies that bubble mobility and sweeping phenomena do not necessarily determine the fission gas behavior. This again is in agreement with experimental observations. The slow mobility of the bubbles is probably due to a contamination of the bubble surfaces with solid fission products which makes the bubbles move via volume diffusion of the lattice atoms rather than by (the faster process of) surface diffusion.

In summary, the model is seen to adequately describe the gas behavior in oxide fuels where the bubbles do not grow indefinitely but rather reach a constant size.

In Appendices V to IX, a more extensive variation of the parameters,  $D$ ,  $a$ ,  $n$ , and  $\eta$  is presented. Such a parametric study together with a confrontation with post-irradiation examinations is hoped to allow a satisfactory definition of the two basic parameters,  $D$  and  $\eta$ , which are difficult to determine in another way and which cause most of the scatter at the present stage.

REFERENCES

- 1) A.H. Booth and G.T. Rymer, Chalk River (Canada) Report CRDC-720 (1957)
- 2) R. Lindner and Hj. Matzke, Z. Naturforschg. 13a (1958)<sup>794</sup> and 14a (1959) 582 and 1074
- 3) J.R. MacEwan and W.H. Stevens, J. Nucl. Mat. 11 (1964) 77
- 4) A.D. Whapham, Nucl. Applications 2 (1966) 123
- 5) J.R. MacEwan and P.A. Morel, Nucl. Applications 2 (1966) 158
- 6) Hj. Matzke, Nucl. Applications 2 (1966) 131
- 7) M.E. Gulden, J. Nucl. Mat. 23 (1967) 30
- 8) R.M. Cornell, Phil. Mag. 19 (1969) 539
- 9) R.S. Barnes and R.S. Nelson, Harwell (U.K.) Report AERE-R 4952 (1965)
- 10) F.A. Nichols, J. Nucl. Mat. 27 (1968) 137 and 30 (1970) 143
- 11) D.J. Clough, J.R. Findlay, R.S. Nelson, J.B. Rich, J.B. Sayers, and A.D. Whapham, Symp. Rad. Dam. in Reactor Materials IAEA Vienna, paper SM-120/G-2 (1969).
- 12) A.M. Ross, J. Nucl. Mat. 30 (1970) 134
- 13) R.M. Cornell, M.V. Speight and B.G. Masters, J. Nucl. Mat. 30 (1970) 170
- 14) M.V. Speight, Nucl. Sci. Eng. 37 (1969) 180
- 15) Hj. Matzke, Physics of Ionized Gases, Proc. Int. Summer School Herceg-Novci, Ed. B. Navinšek, Ljubljana (1970) p. 354
- 16) Various articles in the August issue of Nucl. Appl. Technol. 9, (1970) 127 to 218
- 17) F.S. Ham, J. Phys. Chem. Solids 6 (1968) 335
- 18) M. Coquerelle, L. Koch and C. Ronchi, Proc. ANS Meeting, Fast Reactor Fuel and Fuel Elements, p. 411, Karlsruhe (1970)
- 19) e.g. R.M. Cornell, M.V. Speight, and B.C. Masters, J. Nucl. Mat. 30 (1969) 170
- 20) R.S. Nelson, J. Nucl. Mat. 31 (1969) 153
- 21) Hj. Matzke, Semiannual progress report TUSR-11 (1971)
- 22) C. Ronchi and Hj. Matzke, Trans. ANS 14,2(1971)580
- 23) R.M. Coquerelle, personal communication
- 24) J.A. Turnbull, UK Report RD/B/N1112 (1968)
- 25) J.A. Turnbull and R.M. Cornell, J. Nucl. Mat. 36 (1970) 161 and 41 (1971) 156
- 26) S. Cavaleru, PhD Thesis, University of Salford, (1971)
- 27) H. Blank and Hj. Matzke, in print (1972)

List of symbols

$\Delta V$	precipitation volume, assumed to be spherical, surrounding each bubble nucleus, $\text{cm}^3$
$\rho$	radius of $\Delta V$ , cm
$r_0$	bubble radius, cm
$c$	concentration of gas in atomic (dynamical) solution, mole $\text{cm}^{-3}$
$g$	concentration of gas at grain boundaries, mole $\text{cm}^{-3}$
$b$	concentration of gas in intragranular bubbles, mole $\text{cm}^{-3}$
$c^*$	concentration of gas that is <u>not</u> precipitated in a bubble, mole $\text{cm}^{-3}$
$c_1$	concentration of gas in thermal solution, mole $\text{cm}^{-3}$
$m$	number of gas atoms in an individual bubble, mole
$c_0$	$c - c_1$ , mole $\text{cm}^{-3}$
$\phi$	net flux of gas atoms through the surface of $\Delta V$ , mole $\text{cm}^{-3} \text{sec}^{-1}$
$\tau_0$	relaxation time for precipitation, sec
$n$	concentration of bubbles, $\text{cm}^{-3}$
$\beta$	production rate of gas atoms, mole $\text{cm}^{-3} \text{sec}^{-1}$
$\Gamma$	resolution rate, mole $\text{sec}^{-1}$
$d$	thickness of bubble shell subjected to resolution, cm
$\eta$	resolution probability for a given gas atom, $\text{sec}^{-1}$
$E$	critical energy for resolution, eV
$b$	Van der Waals constant, $\text{cm}^3 \text{mole}^{-1}$
$\dot{s}$	fission rate, $\text{cm}^{-3} \text{sec}^{-1}$
$\gamma$	surface tension of solid, $\text{dyn cm}^{-1}$
$R$	gas constant, $\text{erg } ^\circ\text{K}^{-1} \text{mole}^{-1}$
$T$	temperature, $^\circ\text{K}$
$D$	effective diffusion coefficient for mobility of single gas atoms, $\text{cm}^2 \text{sec}^{-1}$
$a$	grain size in fuel microstructure, cm
$t$	irradiation time, sec
$K$	differential precipitation constant, $\text{sec}^{-3/2}$
$C$	differential resolution constant, $\text{sec}^{-1}$

Appendix I : Derivation of the precipitation laws

Here, we want to derive the solution for precipitation of gas from a super-saturation into bubbles in the absence of irradiation. Hence, we want to solve the diffusion equation (see Section 2.1) :

$$\frac{\partial c}{\partial t} = - D \nabla^2 c \quad (\text{I-1})$$

with the boundary conditions

$$c(r_0) = c_1, \text{ and} \quad (\text{I-1a})$$

$$\left. \left( \frac{\partial c}{\partial r} \right) \right|_{r=r_0} = 0 \quad (\text{I-1b})$$

Here,  $r_0$  is the radius of the bubble and  $r$  the radius of each surrounding (spherical) volume element  $\Delta V$ , influenced by the bubble.

The solution of Equ. (I-1) has the form

$$c = c_1 + \sum_{n=0}^{\infty} a_n(t) \varphi_n(r)$$

where the  $\varphi_n$  are eigenfunctions of the operator  $\nabla^2$  with eigenvalues  $\lambda_n^2$ .

Hence

$$\frac{da_n(t)}{dt} = -D \lambda_n^2 a_n(t) \quad (\text{I-2})$$

since the  $\varphi_n$  are orthogonal functions.

From Equ. (I-2) follows

$$c \approx c - c_1 = \sum_{n=0}^{\infty} a_n^0 \exp(-t/\lambda_n^2 D) \varphi_n$$

with

$$a_n^0 = \int_V [c - c_1]_{t=0} \varphi_n \, d\vec{r}.$$

For the above case, the  $\varphi_n$ 's have a simple form :

$$\varphi_n = A_n \exp \left\{ -i \lambda_n (r - r_0) \right\}$$

and therefore, with Equ. (I-1a)

$$\varphi_n = A_n \frac{\sin \lambda_n (r-r_0)}{r}$$

Since because of Equ. (I-1b)

$$\left(\frac{\partial \varphi_n}{\partial r}\right)_{r=\varrho} = 0,$$

the equations for the eigenvalues are easily obtained

$$\operatorname{tg} \lambda_n (r-r_0) = \lambda_n \varrho.$$

For the case of  $\varrho \gg r_0$ , i.e. a small bubble concentration, one obtains

$$\lambda_0^2 = 3 r_0 / \varrho^3, \text{ and}$$

$$\varphi_0 = \lambda_0 A_0 (1-r_0/r).$$

The values  $\lambda_n$  are larger and can eventually be approximated to  $(2n+1)\pi/4\varrho$ , i.e. the functions  $\varphi_n$  ( $n > 0$ ) represent solutions that disappear very fast with increasing irradiation time,  $t$ .

We still want to determine the values of  $a_n$  and  $A_n$ .

If at  $t = 0$ ,  $c = c_1 + c_0$  (see Fig. 1b), we obtain

$$a_n = \int_{\Delta V} c_0 \varphi_n dr = \int_{r_0}^{r_1} c_0 A_n \sin \lambda_n (r-r_0) r dr \cdot 4\pi = \frac{4\pi c_0 A_n r_0}{\lambda_n}$$

$$\text{Hence } A_n^2 = \frac{2}{4\pi \lambda_n^2} \cdot \frac{(1+\lambda_n^2 \varrho^2)}{\varrho^2 (\varrho-r_0)-r_0} \quad (\text{I-3})$$

This implies, that the terms for larger values of  $n$  decrease very rapidly. Already the term for  $n = 1$  represents  $\leq 1\%$  of  $c$  for values of time of about  $\tau_0 = 1/\lambda^2 D$ . Therefore, we may restrict ourselves on the term with  $n = 0$ .

Thus we get

$$c = \frac{c_0 \rho^3}{3r_0 r} \exp(-t/\tau_0) \sin \left\{ (r-r_0) \frac{3r_0}{\rho^3} \right\}$$

Near to the bubble surface, where  $r - r_0 \approx 0$ ,  $c$  is given by

$$c \approx c_0 \exp(-t/\tau_0) (1-r_0/r) \quad (\text{I-4a})$$

and far away from the bubble, hence for  $r \gg r_0$

$$c \approx c_0 \exp(-t/\tau_0). \quad (\text{I-4b})$$

Appendix II : On the choice of the resolution parameter.

The dynamical resolution of the fission rare gases krypton and xenon due to interaction with fission spikes which is known to cause a certain solubility of the gas and which may lead to the destruction of bubbles during irradiation (4) can occur via two mechanisms :

- a) either by direct energy transfer to the gas atoms from fission products or from lattice atoms belonging to the related collision cascades, or
- b) by a "sputtering" mechanism which consists in the ejection of material by fission spikes from one side of the bubble thus burying gas atoms on the other side.

Direct collisions of precipitated gas atoms with fast neutrons are much less effective (24) and can be neglected.

In the following, we want to calculate the resolution due to process a). The quantity characterizing any resolution process is the probability,  $b$ , per second of a gas atom being dissolved from a bubble. This probability is determined by

- i) the probabilities  $\eta'$  and  $\eta''$  to gain more energy than a certain minimum energy,  $E_{\min}$ , by collisions with either fission fragments ( $\eta'$ ) or with lattice atoms ( $\eta''$ ) of the collision cascades
- ii) the probability of the gas atom to remain stuck in the lattice and not be reflected or desorbed instantaneously, i.e. the sticking factor  $S$ ,

iii) at higher temperatures, the probability  $d$  of the gas ending up in an equilibrium position for a volume diffusion process. Gas atoms located very near to surfaces, in contrast, frequently are desorbed at low temperatures.

To calculate  $\eta$ , we thus need to know  $S$ ,  $d$ ,  $\eta'$  and  $\eta''$ .

The quantities  $\eta'$  and  $\eta''$  can be calculated (20), and transformed into a quantity

$$\psi = - \frac{d(\eta' + \eta'')}{dE_{\min}}$$

which is more useful since it gives directly the probability per unit time of an individual gas atom to attain an energy between  $E$  and  $E+dE$ . The calculated energy dependence of  $\psi$  (for a fission rate of  $10^{13}$  f/cm<sup>3</sup>sec) and the measured (15,26) energy dependences of  $S$  and  $d$  are shown in Fig. II-1 for UO<sub>2</sub>.

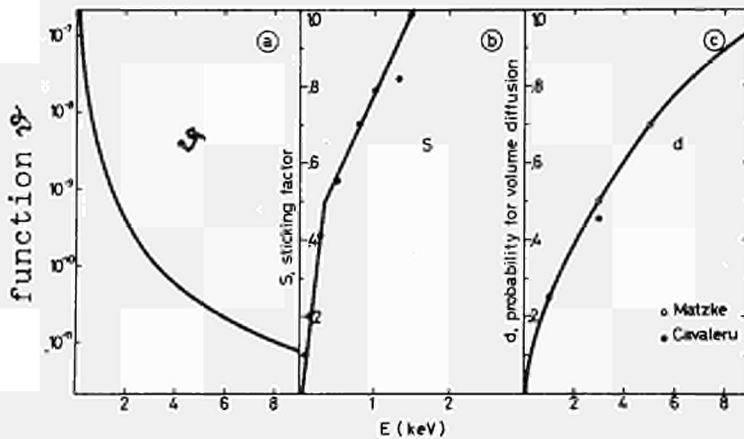


Fig. II-1 Energy dependence of the three factors  $\psi$ ,  $S$ , and  $d$  contributing to the resolution probability for fission gases in oxide fuels.

With this basic information, we can now calculate  $\eta$  for both low and high temperature irradiation by choosing adequate analytical expressions for  $\psi$ ,  $S$ , and  $d$ , and integrating over appropriate energy intervals. In this way, we obtain

$$\eta_{\text{low temp}} = \int_0^{\infty} \psi(E) S(E) dE \approx 5.4 \times 10^{-5} \text{ sec}^{-1}$$

$$\eta_{\text{high temp}} = \int_0^{\infty} \psi(E) S(E) d(E) dE \approx 3.2 \times 10^{-6} \text{ sec}^{-1}$$

The calculated values can be compared to experimental data measured at Berkeley (24,25) by observing threshold fission doses adequate to destroy preformed bubbles. The results are

$$\begin{aligned} 2.6 \times 10^{-5} \leq \eta \leq 1.2 \times 10^{-4} \text{ sec}^{-1} & \text{ at } 200^{\circ}\text{C} \\ 1.8 \times 10^{-4} \leq \eta \leq 3.6 \times 10^{-4} \text{ sec}^{-1} & \text{ at } 1200^{\circ}\text{C} \end{aligned}$$

From this, we conclude that the direct or collision mechanism a) might well be effective at low irradiation temperatures since the calculated value falls midway into the experimental range. At high temperatures, on the other hand, most of the resolution must be due to mechanism b) or a related process, e.g. to the increased size of the hot (or even molten) zone with the associated stress waves along the fission spike (27).

Since  $\eta$  therefore most probably falls into the range between roughly  $10^{-5}$  to  $10^{-4} \text{ sec}^{-1}$ , most calculations were performed with these values. In addition, however,  $\eta$  was varied in a much wider range for a specific fuel temperature (see Appendix VIII).

### Appendix III : On the choice of the gas diffusion coefficients

The gas diffusion coefficients were taken from a recent summary (15) where the behavior of rare gases in  $\text{UO}_2$  was discussed in terms of a System of Stages which was developed in analogy to the recovery stages observed in e.g. electrical resistivity studies on quenched or irradiated metals. Fig. III-1 shows a systematic presentation of the stages. Similarly to the recovery of metals, the stages are grouped according to their temperatures with respect to those of self-diffusion and are attributed to specific transport processes. Using isochronal annealing programs, the processes can be separated since one goes to completion after the other, at least in principle. In reality, there is frequently still some overlapping. In isothermal experiments, on the other hand, the Stage that should dominate the release at the temperature in question will be overlapped with release due to all other stages that occur at lower temperatures.

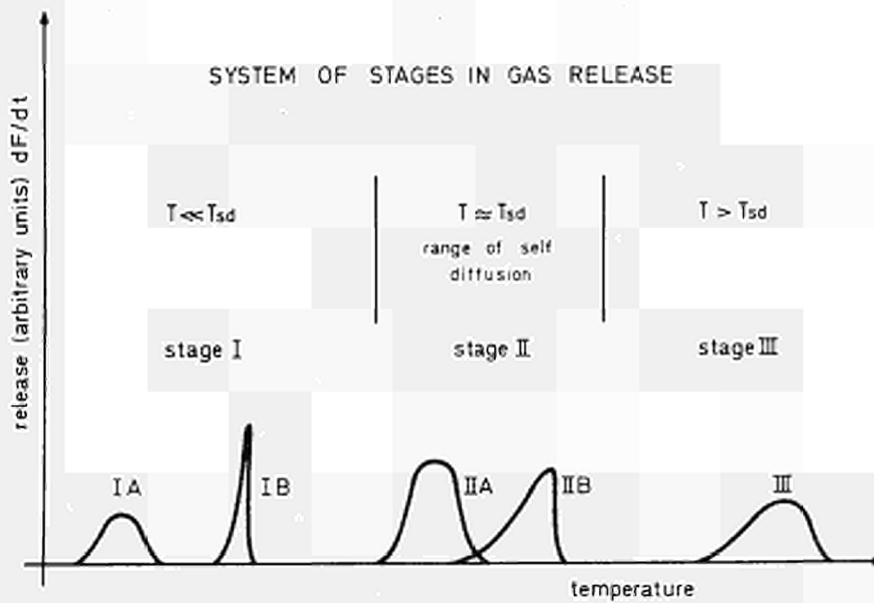


Fig. III-1 Systematic representation of the System of Stages in gas release studies (for the case of a linear temperature increase, i.e.  $dF/dt$  vs temperature).  $T_{sd}$  refers to the temperatures of self-diffusion for the geometrical conditions of the gas release studies (roughly 1100-1700°C for  $UO_2$ )

This is a strong argument in favor of isochronal experiments. Based on results from a variety of systems, it can be shown that.

Stage I involves gas mobility at unusually low temperatures. Stage IA is due to gas fortuitously located in high mobility sites, e.g. in an interstitial position.

Stage IB is due to annealing of structural radiation damage, the most common form of which is radiation induced amorphousness.

Stage II involves gas mobility at normal temperatures, i.e. temperatures similar to those of self-diffusion of the matrix atoms.

- Stage IIA is due to unperturbed mobility of single gas atoms involving vacancies in some kind or another.
- Stage IIB is due to temporary trapping of gas, i.e. to weak interactions of gas atoms with radiation damage or pre-existing defects, or with other gas atoms.
- Stage III involves gas mobility at unusually high temperatures and is due to strong trapping of gas at preexisting defects or in gas-filled bubbles.

The system of Stages in  $UO_2$  is discussed in detail in ref. (15). The most representative data are summarized in an Arrhenius diagram in Fig. III-2. This figure intends to summarize the present state of knowledge of the diffusion of rare gases in  $UO_2$ . The diffusion of single gas atoms or Stage IIA is represented by the area 1, covering the scatter in results. The present authors feel that the upper half of area 1 is most representative for truly undamaged  $UO_2$ . Stage IIB or trapping is covered by area 2, which is expected to be of a finite width due to different types of defects contributing to trapping. At low temperatures and near to the surface, Stage IA sets in as indicated by area 3. During reactor irradiation, the fission rate dependent "diffusion" dominates at lower temperatures, as shown by area 4.

Stage IA mobility is responsible for the decreased re-resolution probability at increased temperatures (see Appendix II). For our present purpose, Stages IIA and B are of more direct interest, in addition to the fission rate dependent diffusion at low temperatures (area 4).

For the calculation, a set of high, medium and low values of  $D$  were chosen from the border lines of area 1 (upper line =  $D_{high}$ ; lower line of area 1 = upper line of area 2 =  $D_{medium}$ ; lower boundary of area 2 =  $D_{low}$ ). A priori,

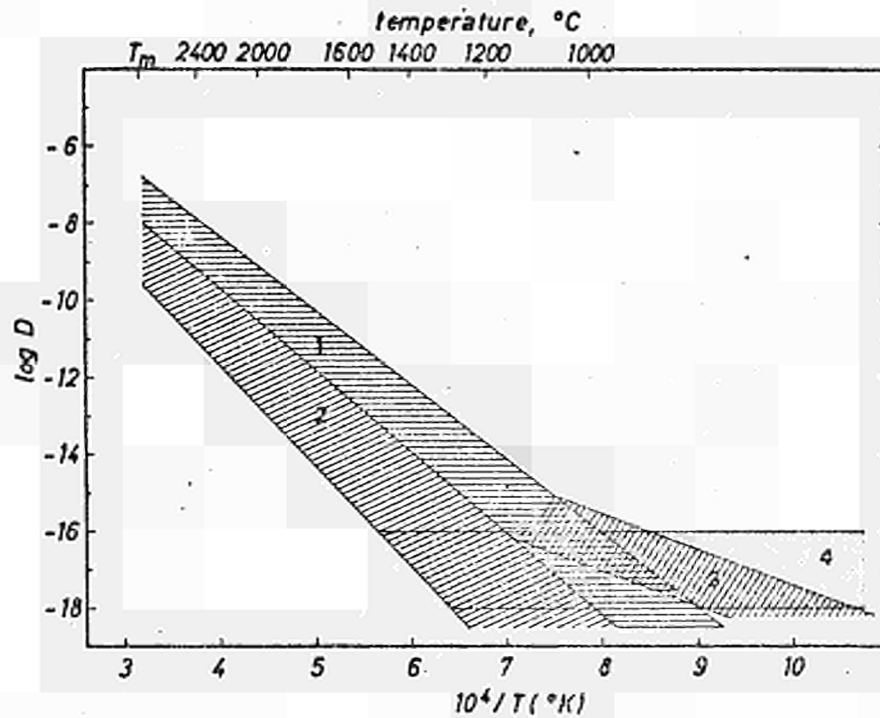


Fig. III-2 Summary of the reliable literature data on the mobility of fission gases in  $UO_2$ , presented in form of an Arrhenius diagram. Area 1 represents the scatter in results on Stage IIA diffusion, i.e. mobility of single gas atoms, area 2 shows Stage IIB or trapping of gas. At low temperatures, Stage IA or surface effects are dominating (area 3) whereas during reactor irradiation the fission events cause a "mixing" of atoms as a type of radiation enhanced diffusion which depends on the fission rate but not on the temperature (area 4).

a decision on what set of data is most representative for high irradiation levels is difficult to make. The  $D_{high}$  values correspond to undamaged material, whereas the  $D_{low}$  values represent high burn-up material in out-of-pile release studies. If there is any re-resolution effect on trapped gas atoms, similar to the re-resolution of gas atoms from bubbles, then values near to  $D_{medium}$  should be most representative for in-pile conditions. The present model calculations are hoped to settle this question by comparing the calculated results on bubble formation and release with experimental ones (see also Section 3.4).

Appendix IV : Model simplified with the assumption that all gas atoms are trapped in intra-granular bubbles before being released

A slightly simplified version of the presented model is obtained, if all gas atoms are assumed to be trapped in bubbles before they, following resolution, are able to diffuse towards grain boundaries. Though such a model (model A in Fig. IV-1) is physically less satisfactory than the model described in the text (model B in Fig. IV-1, see also Fig. 2), where some gas atoms created near the grain boundary can escape without ever being trapped in a bubble,

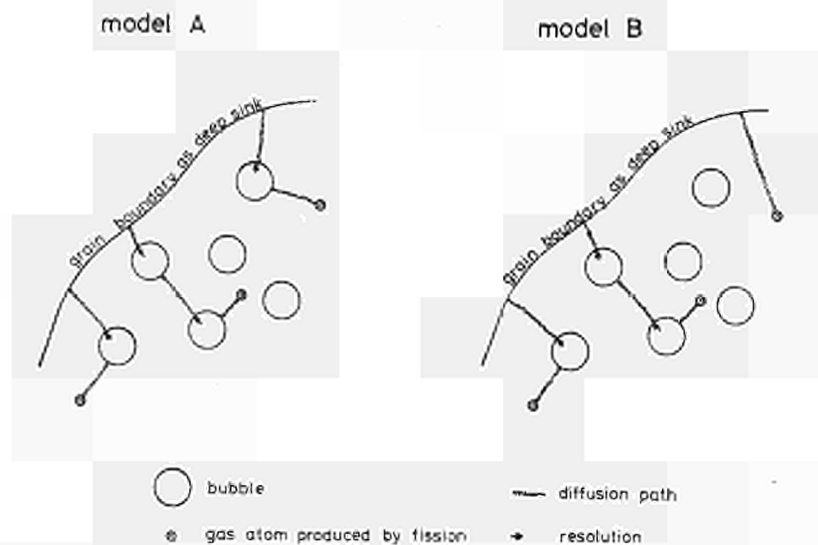


Fig. IV-1 : Sketch illustrating the assumptions on transport of fission gas atoms towards grain boundaries

it seems worthwhile to briefly mention the differences brought about by such a change in the model. As expected because of the high bubble density and the big grain sizes employed, the changes do not appreciably affect the practical implications of the model but they are interesting for the basic understanding of fission gas behavior.

In the simplified model, the basic system of differential equations is easier to treat than equ. (7) since the square bracket in the expression for  $dg/dt$  in equ. (7) can be replaced by

$$\left[ 1 - \frac{6}{\pi^2} \sum_{n=1}^{\infty} \frac{1}{n^2} \exp(-n^2 \pi^2 Dt/a^2) \right]$$

and a short time solution can be obtained :

$$\frac{dc}{dt} = - \frac{(K \sqrt{t} + C + G(1+Ct)/\sqrt{t})c}{1 + 2G\sqrt{t}} + \frac{B(1+Ct)}{1+2G\sqrt{t}}$$

where  $K$  and  $C$  are as in equ. (7) and  $G = 3/a (D/\pi)^{1/2}$

In this case, both the concentration of gas in bubbles,  $b$ , and at grain boundaries,  $g$ , increase linearly with the irradiation time. Therefore, it would a priori not be possible to predict which of the two competitive mechanisms of swelling and gas release would dominate. This would rather depend on the fuel and irradiation parameters. It seems worth remarking that the concentration of bubbles,  $b$ , and thus also the swelling coefficient do not reach a saturation value as they do in model B.

In contrast,  $c$  increases asymptotically with the square root of time. This is indicated in Fig. IV-2 (dashed lines) where also the behavior according to the physically more realistic model B (full lines) is shown. The effect of a variation of bubble density (increase by a factor of 100) or re-solution probability (reduced by a factor of 10) is shown in Fig. IV-3 (see also Appendix VII for a similar variation for model B). Again, the same asymptotic behavior is noted, according to the approximate solution for large values of  $t$  of the above equation :

$$c_{\infty} = C \beta \sqrt{t} / K$$

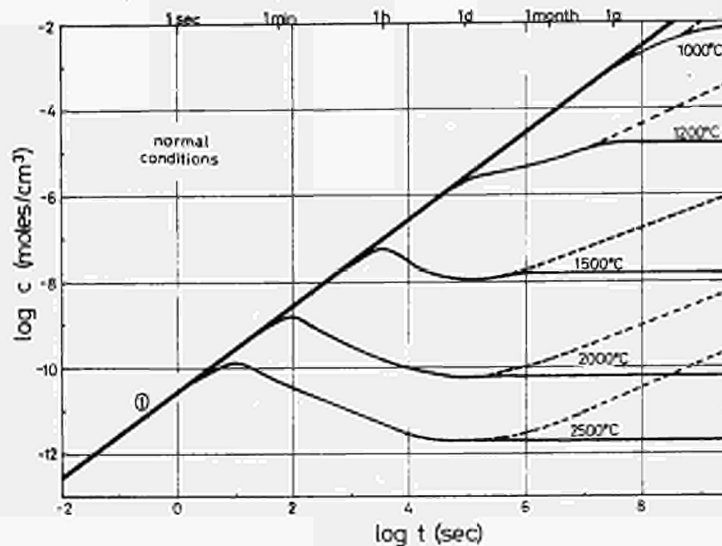


Fig. IV-2 Fission gas concentration,  $c$ , in dynamical solution for the conditions of Table I (see page 13) and for different temperatures. Line 1 represents the production of the rare gas by fission. The full curves are for model B (see also Fig. 3 on page 15), the dashed curves are for model A.

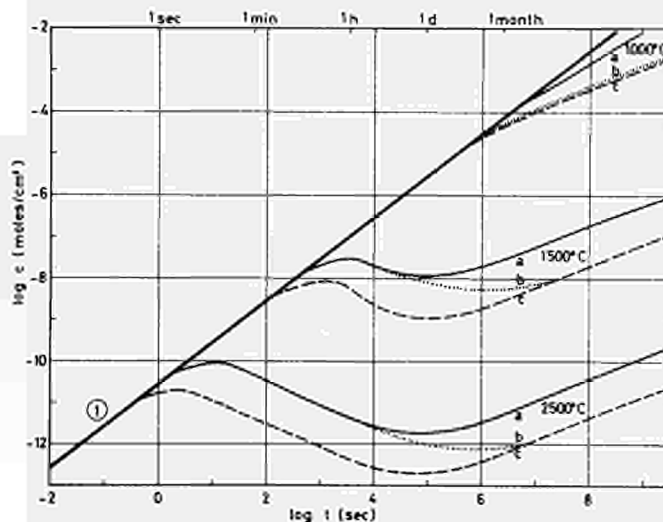


Fig. IV-3 As Fig. IV-2, but all curves for model A. Curves a correspond to the dashed curves of Fig. IV-2; Curves b are for an increase in bubble density by a factor of 100 and curves c are for a reduced re-resolution probability (by a factor of 10).

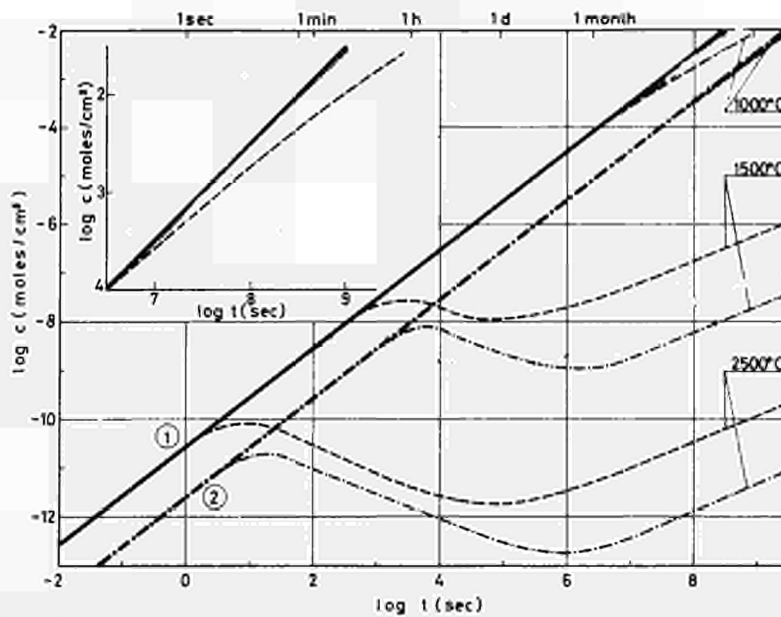


Fig. IV-4 As in Fig. IV-2, but in addition, calculations for typical thermal reactor conditions (see Appendix V) are given. All curves are for normal conditions (----and line 1 = fast reactor; - - - - and line 2 = thermal reactor ).

In Fig. IV-4, finally, a comparison is made between fast flux conditions (high fission rate, i.e. high value of  $\beta$ ) and thermal conditions (smaller  $\beta$ , see Appendix V). In the insert of Fig. IV-4, the calculations for 1000°C are shown on a bigger and extended scale\*.

\* One should note here and in similar figures in the following appendices, that such extensions to high values of  $t$  are shown only to demonstrate the mathematical trend of the curves. In reality, such values would correspond to unrealistic situations. The calculations are thought to be realistic up to  $t \approx 10^7$  to  $10^8$  sec.

### Parametric study

In the following appendices V to IX, results of an extensive parametric study will be presented.

Both typical thermal reactor conditions (Appendix V) and fast flux conditions (Appendices VI to IX) will be considered. Specifically, the following parameters will be varied in addition to varying the fuel temperature

- the gas diffusion coefficient,  $D$
- the bubble density,  $n$
- the re-resolution probability,  $\eta$
- the grain size,  $a$ .

Appendix V : Thermal reactor conditions

The following conditions (see Table V-1) were selected for thermal reactor irradiations : the quantities depending on the fission rate, i.e. the gas production rate and the resolution probability,  $\eta$ , were both decreased by a factor of 10 as compared to fast flux conditions. The microstructure (grain size,  $a$ ) and the bubble density,  $n$ , remained unchanged. For the gas diffusion coefficients, values called previously  $D_{norm}$  were chosen with the exception of 1000°C, where because of the smaller fission rate and the fact that at 1000°C the radiation enhanced diffusion is expected to contribute to the gas mobility, a lower  $D$  value was chosen (see Table V-1).

Some results have already been shown in Fig. IV-4 where  $c$  is compared for fast and thermal conditions. Similar curves for the improved model are shown in Fig. V-1. Essentially, all curves for the thermal reactor are shifted to higher values of time because of the decreased value of  $\beta$ . Due to the decrease in  $\eta$ ,  $c$  is always smaller in the thermal reactor (by about a factor of 10).

Table V-1

Parameters for thermal reactor conditions

Temperature	$D_{norm}$ ( $cm^2 sec^{-1}$ )	$a$ $\mu m$
1000	$1.5 \times 10^{-18}$	10
1500	$5 \times 10^{-12}$	20
2500	$3 \times 10^{-8}$	100

$$\beta = 2.9 \times 10^{-12} \text{ moles } cm^{-3} \text{ sec}^{-1}$$

$$n = 10^{14} \text{ cm}^{-3}$$

$$\eta = 1.9 \times 10^{-6} \text{ sec}^{-1}$$

$$\gamma = 10^3 \text{ erg } cm^{-2}$$

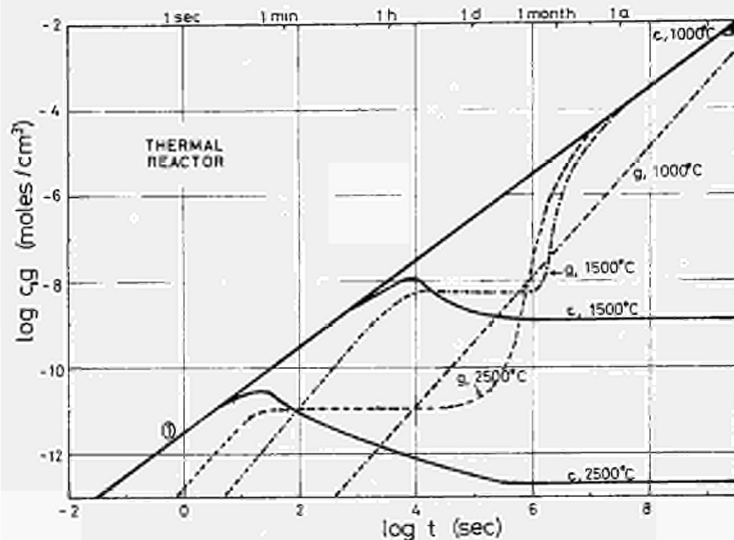


Fig. V-1 Fission gas concentrations,  $c$ , in dynamical solution (full lines) and  $g$ , precipitated at grain boundaries (broken lines) for three fuel temperatures and the thermal reactor conditions of Table V-1. Line 1 represents the production of the rare gas by fission.

Fig. V-1 contains also the time dependence of the concentration of gas which precipitated at grain boundaries. Similar curves are discussed in more detail in Appendix VI. Essentially,  $g$  is seen to increase at small values of  $t$  until it reaches a temporary saturation due to the simultaneous onset of precipitation of gas into bubbles. Only when this part of the gas reaches its saturation value due to continuous re-solution,  $g$  increases again. In its asymptotic behavior,  $g$  is seen to approach the line 1, i.e.  $Bt$ , except for low fuel temperatures (see curve for 1000°C), where such a behavior would mathematically not be expected even at unrealistically high values of  $t$ .

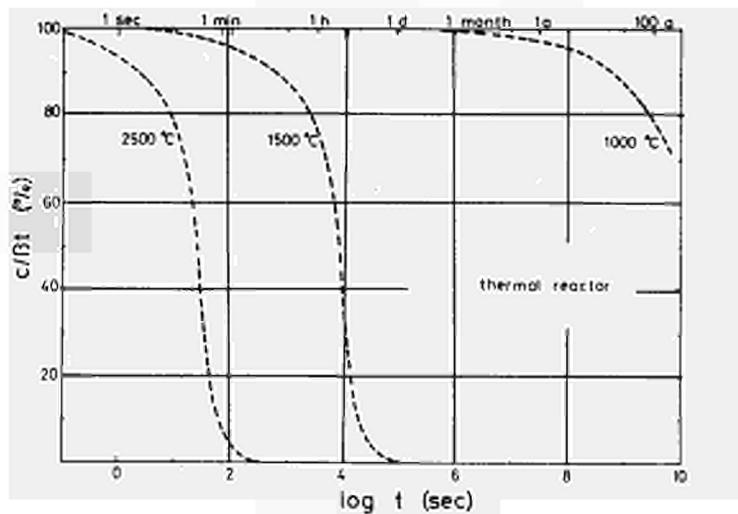


Fig. V - 2 Percentage of fission gas in dynamical solution for three different temperatures and the thermal reactor conditions of Table V-1.

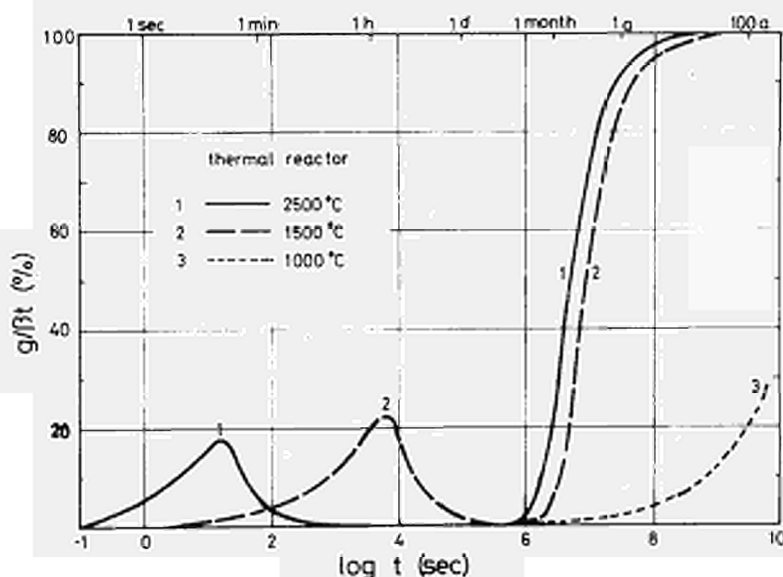


Fig. V - 3 Percentage of fission gas precipitated at grain boundaries for three different temperatures and the thermal reactor conditions of Table V-1.

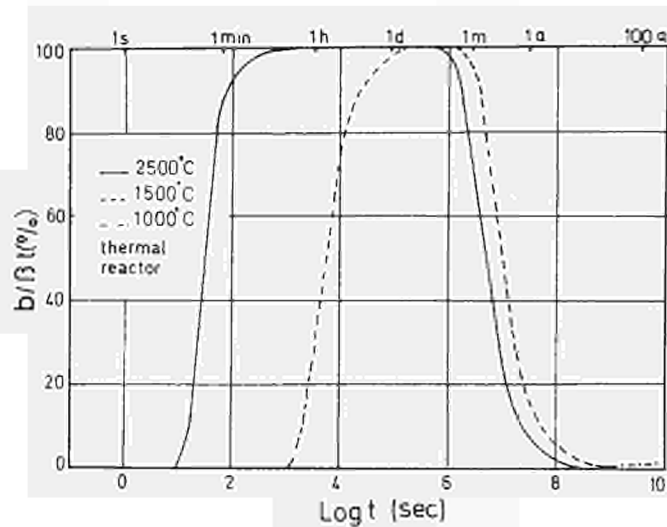


Fig. V- 4 Percentage of gas precipitated into intragranular bubbles,  $b/Bt$ , for three different temperatures and the thermal reactor conditions of Table V-1

Figs. V-2 to V-4 show the percentages of gas in solution,  $c$ , at grain boundaries,  $g$ , and in intragranular bubbles,  $b$ , for three different fuel temperatures of 1000, 1500, and 2500°C calculated for the parameters of Table V-1. At 1000°C, practically all the gas stays in solution for reasonable values of time ( $c \approx 97\%$  at  $t = 1a$ , where  $b$  is still  $< 1\%$  and the remaining gas has reached the grain boundaries).

In this way of presentation, i.e. plotting the percentages rather than the total concentrations, the curves resemble closely those calculated for fast flux conditions with a decreased resolution rate (named  $\eta/10$  in Appendix VII).

Appendix VI: Calculations for fast flux irradiation and different typical fuel temperature

In this appendix, calculations are given for the "normal conditions" of the text together with calculations where the gas diffusion coefficient D was varied. For the "normal conditions", the upper limit of free gas diffusion (Stage II A, see Appendix III) had been chosen, as also indicated in Table VI-1. A second set of calculations was performed with median values of D (see  $D_{med}$  in Table VI-1) which were chosen from the border line of areas 1 and 2 (hence Stages II A and II B) of Fig. III-2 of Appendix III. These values would represent a certain trapping due to higher burn-up and hence radiation damage. Similar calculations for the lower limits of D, referred to as  $D_{low}$ , are given in Appendix VII. These would correspond to final

Table VI-1  
Parameters for calculations in Appendix VI

Temperature (°C)	rad. enhanc. diff.	1000	1200	1500	2000	2500
$D_{norm}$ (cm <sup>2</sup> sec <sup>-1</sup> )	$1 \times 10^{-18}$	$1.5 \times 10^{-16}$	$2 \times 10^{-14}$	$5 \times 10^{-12}$	$1 \times 10^{-9}$	$3 \times 10^{-8}$
$D_{med}$ (cm <sup>2</sup> sec <sup>-1</sup> )	---	$1 \times 10^{-17}$	$2 \times 10^{-16}$	$6 \times 10^{-14}$	$3 \times 10^{-11}$	$1.6 \times 10^{-9}$
a (µm)	10	10	10	20	100	100

$\beta = 2.9 \times 10^{-11}$  moles cm<sup>-3</sup> sec<sup>-1</sup>  
 $\eta = 1.9 \times 10^{-5}$  sec<sup>-1</sup>

$n = 10^{14}$  bubbles /cm<sup>3</sup>  
 $\gamma = 10^3$  erg cm<sup>-2</sup>

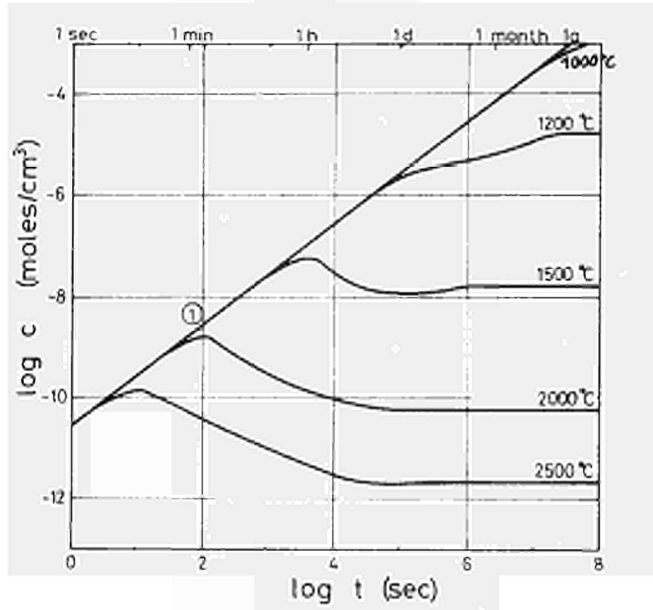


Fig. VI-1 Fission gas concentration,  $c$ , in dynamical solution for the conditions of Table VI-1 (with  $D_{\text{norm}}$ ) and for five different fuel temperatures. Line 1 represents the production of gas by fission.

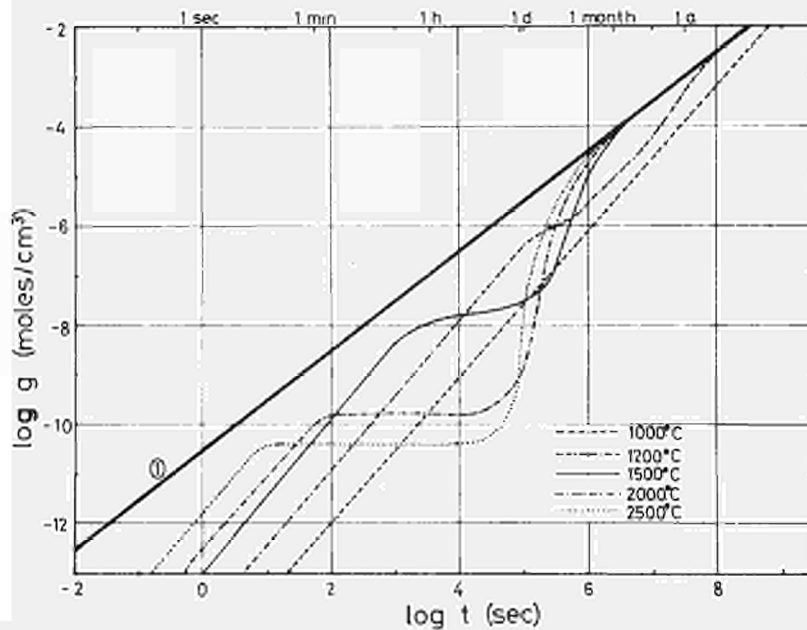


Fig. VI-2 Fission gas precipitated at grain boundaries,  $g$ , for the conditions of Table VI-1 (with  $D_{\text{norm}}$ ) and for five different fuel temperatures. Line 1 represents the production of gas by fission.

trapping as in typical for post-irradiation annealing. If re-resolution affects trapped gas atoms in a similar way as it affects gas atoms precipitated in a gas bubble, the values of  $D_{med}$  could reasonably well represent in-pile conditions.

a) Calculations with  $D_{norm}$

Figs. VI-1 and VI-2 show the time dependence of  $c$  and  $g$  for five temperatures and for radiation enhanced diffusion in a logarithmic scale where again calculated values are shown for very high values of time to indicate the mathematical behavior (even if the corresponding burn-up could never be reached in practice). Figs. VI-3 and 4 show the percentage of  $c$  and  $g$ , and Fig. VI-5 shows the percentage of  $b$  as function of irradiation time. The temporary saturation in  $g$  indicated in the logarithmic plot (Fig. VI-2) corresponds to the maxima in  $g/Bt$  on the linear scale (Fig. VI-4).

b) Calculations with  $D_{med}$

The corresponding results for  $c$ ,  $g$ , and  $b$  calculated with intermediate values of the gas diffusion coefficients,  $D_{med}$ , are shown in Figs. VI-6 to 8. All other parameters were the same for these two sets of calculations.

A comparison of the results shows that the decrease in  $D$  leads to a shift of all curves towards higher values of time though differences of practical interest are evident mainly for low fuel temperatures. This is indicated in the following table VI-2 which gives the values of  $c$ ,  $g$ , and  $b$  for irradiation times of one month and one year, respectively, corresponding to about 1 and 12 a/o burn-up. The values for  $D_{norm}$  are always given first, whereas the values for  $D_{med}$  are given in brackets. Obviously, at one month, the behavior at 2500°C, and at one year, the behavior above 2000°C are practically identical for both sets of  $D$ -values.

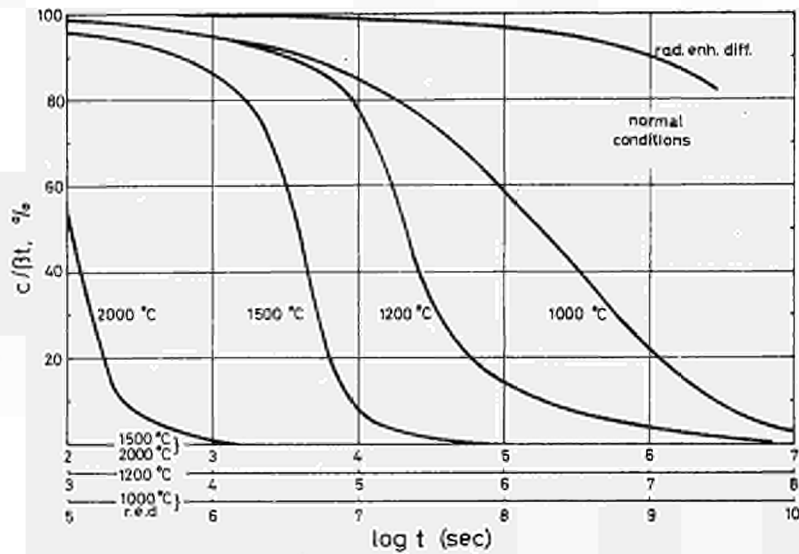


Fig. IV-3 Percentage of fission gas in dynamical solution for the conditions of Table VI-1 (with  $D_{norm}$ ) and for for different fuel temperatures as well as for radiation enhanced diffusion.

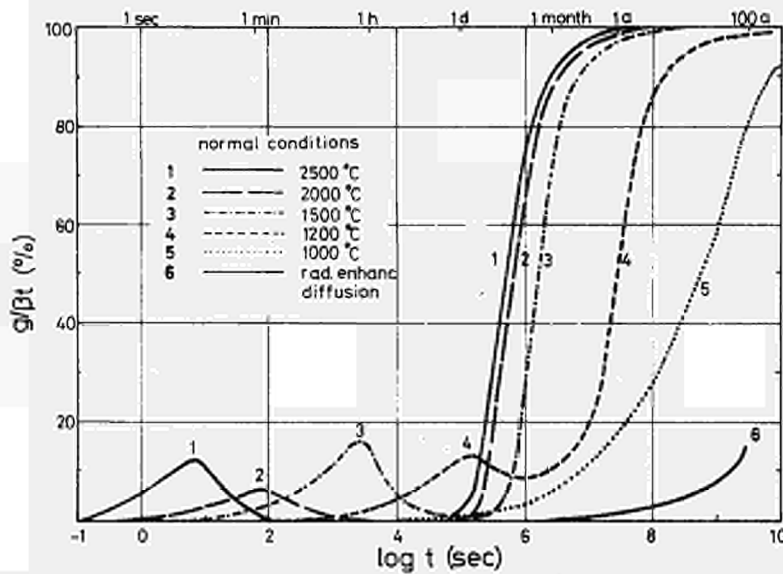


Fig. VI-4 Percentage of fission gas precipitated at grain boundaries for the conditions of Table VI-1 (with  $D_{norm}$ ) and for five different fuel temperatures as well as for radiation enhanced diffusion.

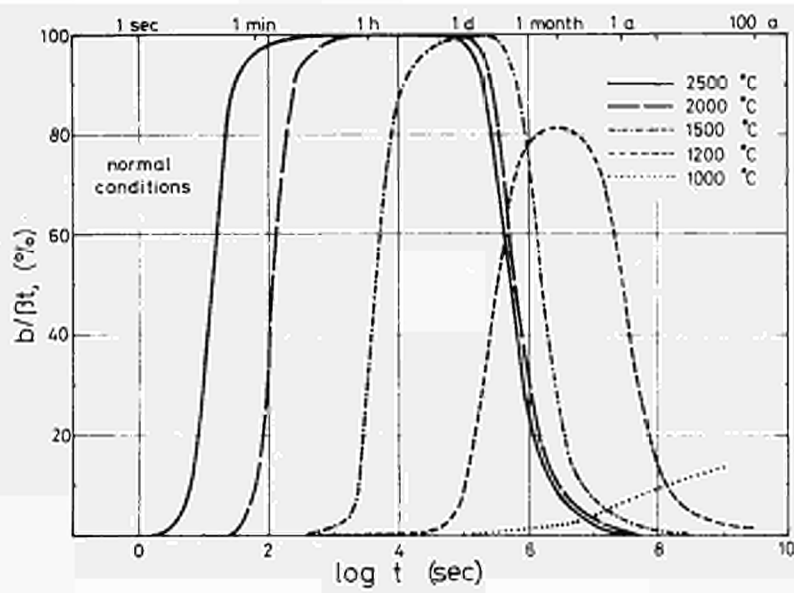


Fig. VI - 5 Percentage of fission gas precipitated in intragranular bubbles for the conditions of Table VI-1 (with  $D_{norm}$ ) and for five different fuel temperatures.

Table VI-2 : Percentages of c, g, and b for  $D_{norm}$  and  $D_{med}$

T	after 1 month			after 1 year		
	c	g	b	c	g	b
1000	92 (100)	6 (~0)	2 (~0)	75 (97)	17 (3)	8 (0)
1200	9 (89)	10(7)	81(4)	2 (71)	47 (22)	49 ( 7)
1500	~0 (3)	70(3)	30(94)	~0 (~0)	96 (16)	8 (84)
2000	~0 (~0)	90(5)	10(95)	~0 (~0)	~98 (89)	~2 (11)
2500	~0 (~0)	92(88)	8(12)	~0 (~0)	~99 (98)	~1 (2)

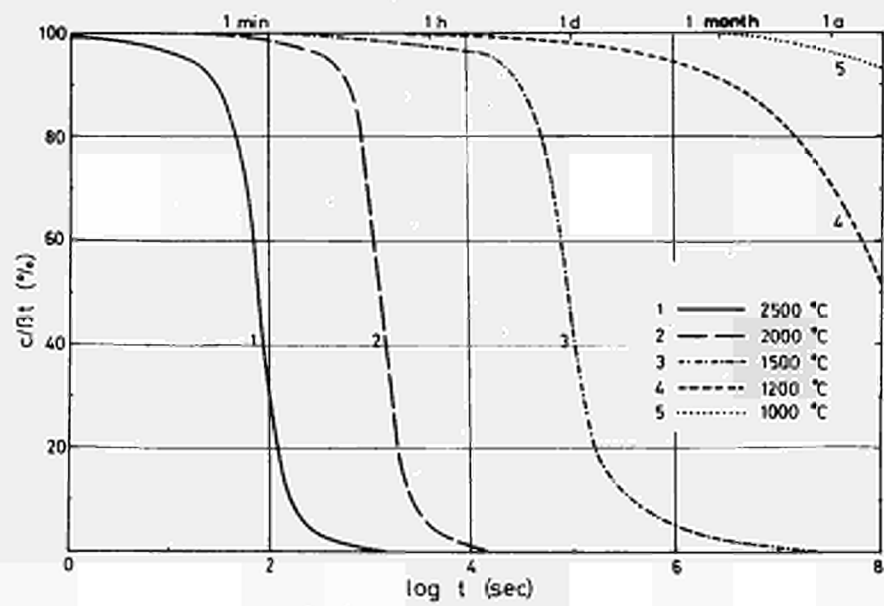


Fig. VI - 6 Percentage of fission gas in dynamical solution for the conditions of Table VI-1 (with  $D_{med}$ ) for five different fuel temperatures

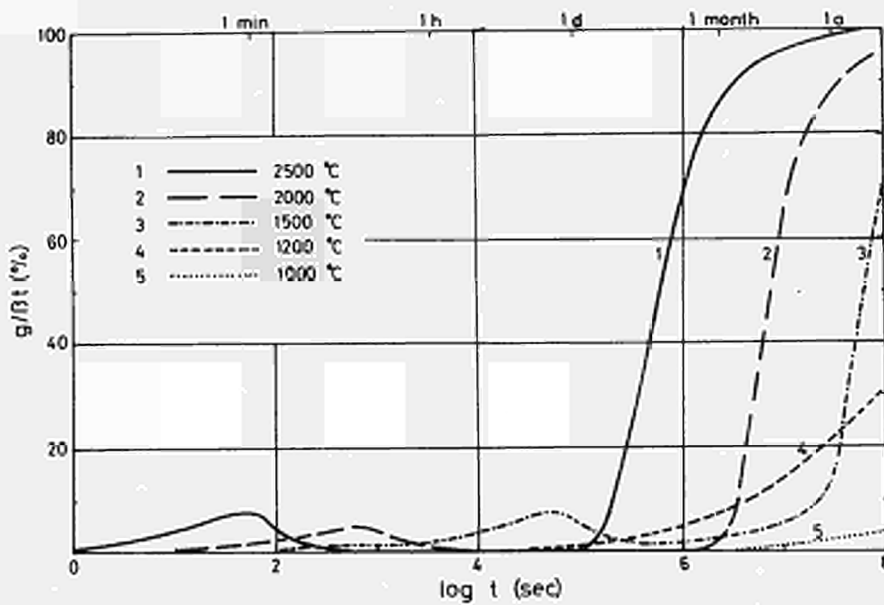


Fig. VI - 7 Percentage of fission gas precipitated at grain boundaries for the conditions of Table VI - 1 (with  $D_{med}$ ) for five different fuel temperatures

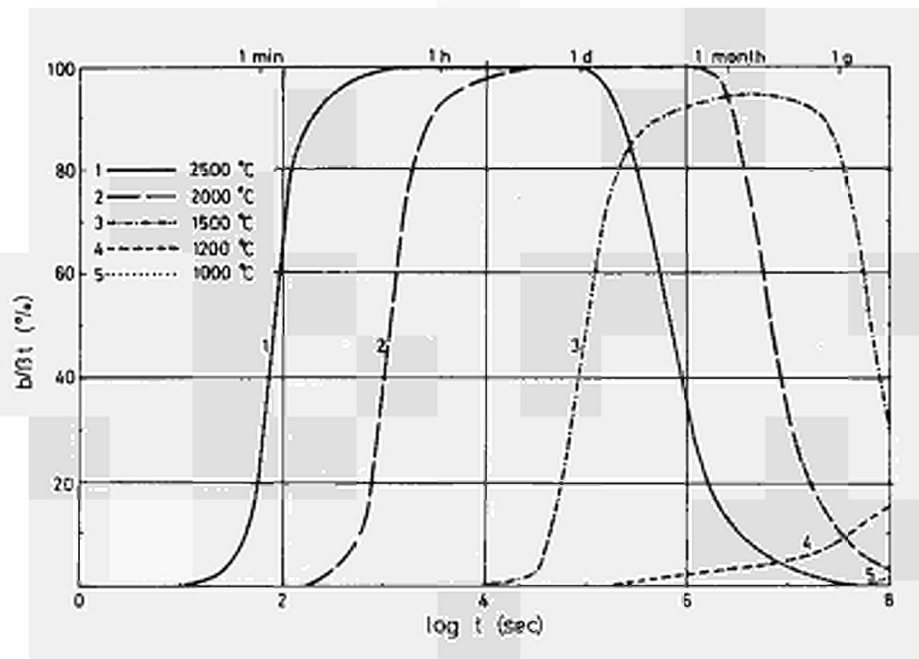


Fig. VI - 8 Percentage of fission gas precipitated in intragranular bubbles for the conditions of Table VI - 1 (with  $D_{med}$ ) and for five different fuel temperatures.

Appendix VII : Parametric study(D,n, $\eta$ ) for fuel temperatures of 1000°C, 1500°C and 2500°C

In this appendix, we want to present results on the variation of the parameters of

- re-resolution probability,  $\eta$ , decreased by a factor of 10
- bubble density, n, increased by a factor of 100
- gas diffusion coefficient, D, decreased to the lower limit  $D_{low}$  (see Appendix III)

for three characteristic fuel temperatures of 1000, 1500 and 2500°C. The parameters used are therefore those called "normal" in Table VI-1 except as indicated in Table VII-1.

Table VII - 1 Parameters varied in comparison to calculations for "normal conditions"

Temperature (°C)	$D_{low}$ (cm <sup>2</sup> sec <sup>-1</sup> )
rad. enh. diff.	1.0 x 10 <sup>-18</sup>
1000	1.5 x 10 <sup>-18</sup>
1500	1 x 10 <sup>-16</sup>
2500	6 x 10 <sup>-11</sup>

re-resolution probability  $\eta/10 = 1.9 \times 10^{-6} \text{ sec}^{-1}$   
 bubble density  $b \cdot 100 = 10^{16} \text{ bubbles/cm}^3$

The curves for "normal conditions" are always shown for comparison and are labelled with the letter "n".

a) Fuel temperature of 1000°C

The results for a fuel temperature of 1000°C are shown in Figs. VII-1 to 5. The concentration of gas in dynamical solution, c, is always high. A decrease in the re-resolution probability  $\eta$  and an increase in bubble density n lead to practically an identical decrease in c, whereas a decrease in D results in very high

values of  $c$  for all times of practical interest.

This behavior can be understood by considering an approximate relationship for  $c$  at very high values of time,  $t$ , which shows that  $c_{\infty}$  is proportional to  $\eta$  and inverse proportional to  $n^{1/2}$

$$c_{\infty} \div \eta / \sqrt{n}$$

Fig. VII-3 shows that at high burn-up and at low fuel temperatures, the choice of the parameters affects the resulting  $c$ -values quite considerably. In contrast, at higher fuel temperatures (see below),  $c$  is always very small at higher burn-up, quite independently of the choice of the parameters.

The amount of gas precipitated at grain boundaries,  $g$ , (see Figs. VII-2 and 4), and hence the expected release, is quite small at any realistic values of the irradiation time. A variation of the parameters does not affect  $g$  by more than about a factor of 2 to 3 even for high burn-up.

The concentration of gas in intragranular bubbles,  $b$ , never reaches 100 %. A decrease in  $\eta$  or an increase in  $n$  again show a very similar trend. The value of  $b$  is increased by more than a factor of 10 for e.g.  $t = 1$  year. The expected maxima lie at the same value of  $t$ , which, however, is unrealistically high. In practice, therefore,  $b$  is expected to steadily increase and not reach saturation. Even if the curves for  $\eta/10$  and  $b.100$  look similar, one should note, however, that the resulting swelling will be much greater for the case of  $\eta/10$  due to the smaller bubble density.

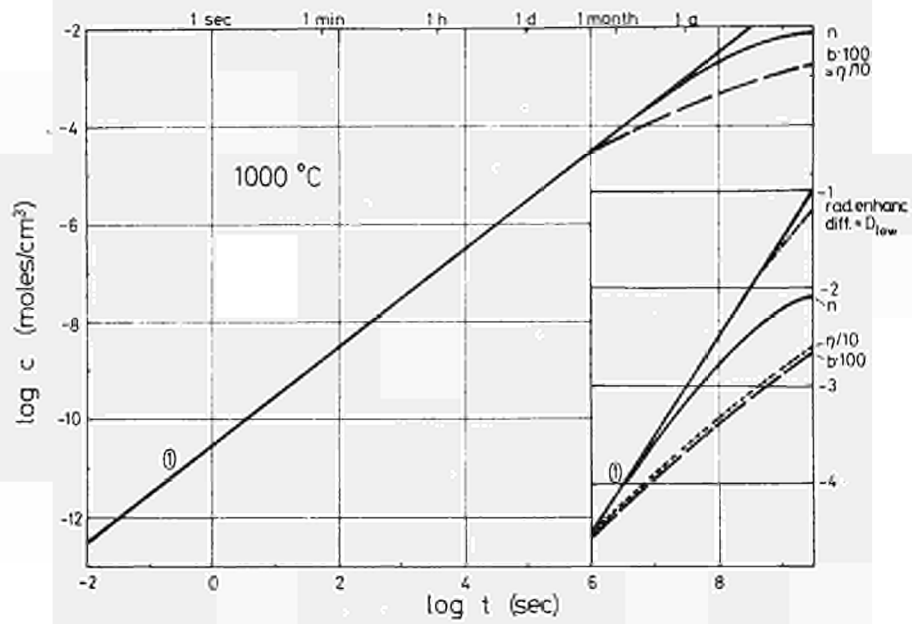


Fig. VII-1 Fission gas concentration in dynamical solution,  $c$ , for a fuel temperature of  $1000^{\circ}\text{C}$  and for radiation enhanced diffusion. For  $1000^{\circ}\text{C}$ ,  $D$ ,  $n$ , and  $\eta$  are varied (see Table VII-1). The part of the curves at high values of  $t$  is shown in a bigger scale in the insert.

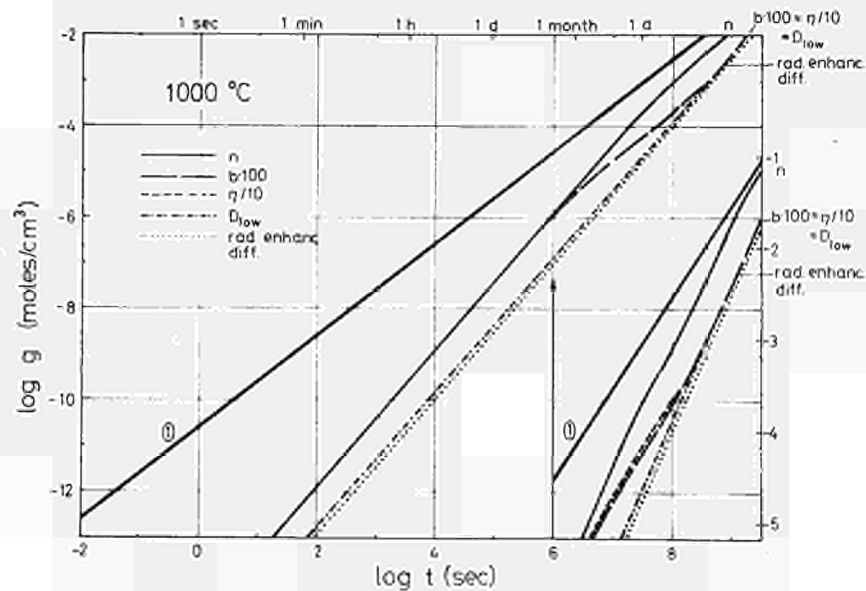


Fig. VII- 2 Concentration of fission gas precipitated at grain boundaries,  $g$ , for a fuel temperature of  $1000^{\circ}\text{C}$  and for radiation enhanced diffusion. For  $1000^{\circ}\text{C}$ ,  $D$ ,  $n$ , and  $\eta$  are varied (see Table VII-1). The part of the curves at high values of  $t$  is shown in a bigger scale in the insert.

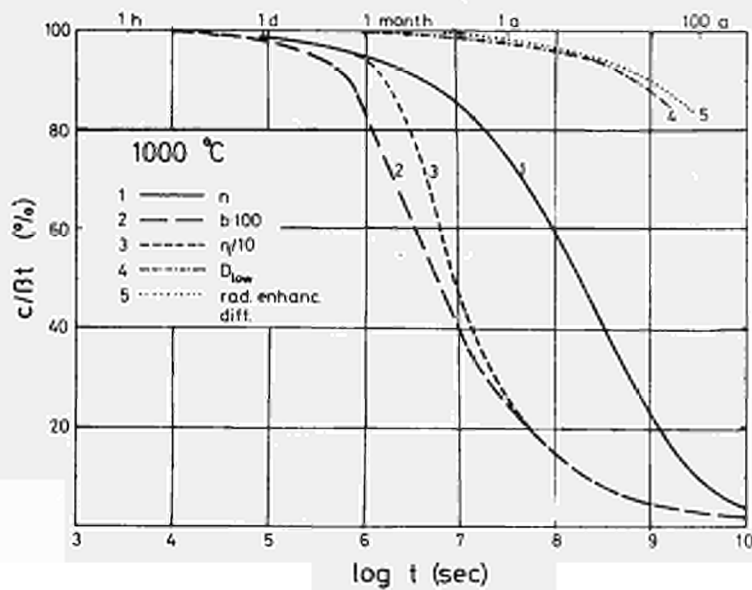


Fig. VII-3 Percentage of fission gas in dynamical solution for a fuel temperature of  $1000^\circ\text{C}$  and for radiation enhanced diffusion. For  $1000^\circ\text{C}$ ,  $D$ ,  $n$ , and  $\eta$  are varied (see Table VII-1)

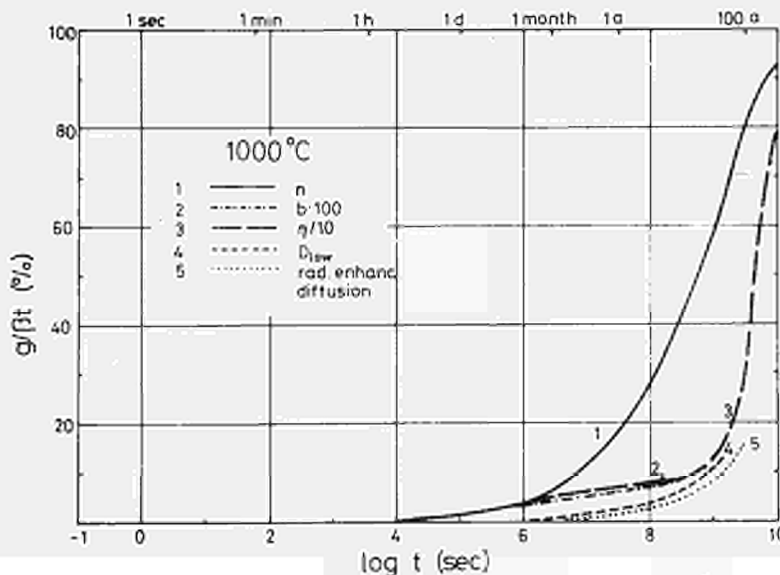


Fig. VII-4 Percentage of fission gas precipitated at grain boundaries for a fuel temperature of  $1000^\circ\text{C}$  and for radiation enhanced diffusion. For  $1000^\circ\text{C}$ ,  $D$ ,  $n$ , and  $\eta$  are varied (see Table VII-1)

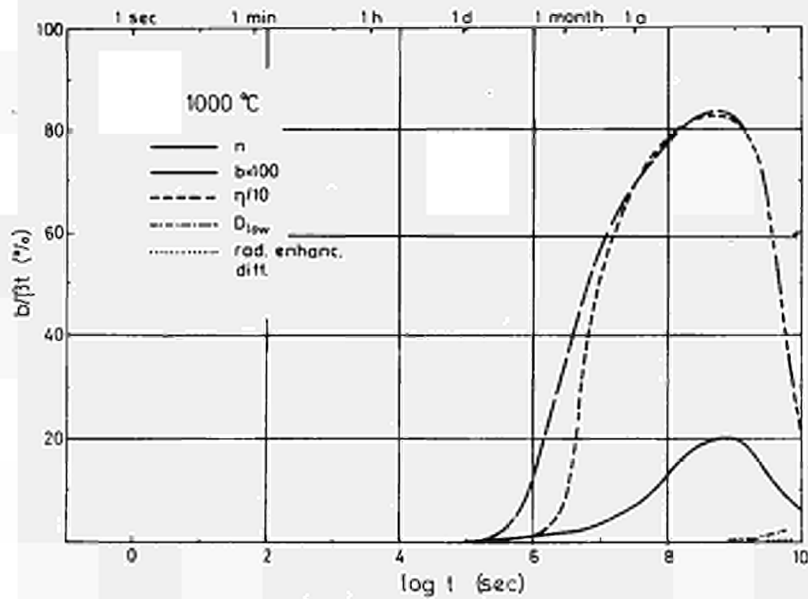


Fig. VII-5 Percentage of fission gas precipitated in intra-granular bubbles for a fuel temperature of 1000°C and for radiation enhanced diffusion. For 1000°C, D, n, and  $\eta$  are varied (see Table VII-1).

It can be shown, that the local, microscopic swelling  $V/V$  is not only proportional b, but also depends on n according to

$$\Delta V/V \div b/n^{3/2}$$

Therefore, going back to Fig. VII-5, swelling will be increased by the above mentioned factor of 10 only for the case of  $\eta/10$ , whereas in the case of b.100, swelling will be different by about  $10/100^{3/2} \approx 0.01$ . This means, that despite of the bigger value of b,  $\Delta V/V$  will be smaller than in the case for "normal conditions".

b) Fuel temperature of 1500°C

The results for a fuel temperature of 1500°C and a variation of  $D$ ,  $n$ , and  $\eta$  are shown in Figs. VII-6 to 11.

The concentration of gas in dynamical solution,  $c$ , (see Figs. VII-6 and 8) is small for any irradiation time of practical interest unless very low values of  $D$  are used. For such low values, the corresponding curve resembles those calculated for  $D_{\text{norm}}$  and 1000°C. In fact,  $D_{\text{norm}}$  at 1000°C (see Table VI-1) is practically identical with  $D_{\text{low}}$  at 1500°C (see also Appendix III) illustrating the unsatisfactory state of the present knowledge on effective in-pile gas diffusion coefficients. The model calculations presented here are hoped to yield a better definition of these values by comparing calculations with experimental results (see below).

The concentration of gas precipitated at grain boundaries,  $g$ , is equally drastically affected by changing  $D$  from  $D_{\text{norm}}$  to  $D_{\text{low}}$ . A change in bubble density by a factor of 100, on the other hand, does not appreciably affect the results, whereas a decrease in  $\eta$  by a factor of 10 shifts the curve for  $g/Bt$  towards higher temperatures by about a factor 10 due to the longer life-time of the gas in bubbles. The maxima in  $g/Bt$  (Fig. VII-9) corresponding to the temporary saturation in  $g$  indicated in Fig. VII-7 are due to free gas diffusion before appreciable bubble growth sets in. They are unimportant in practice since the total amount of gas created is still low at these small irradiation times. It might be noted that for the case of  $D_{\text{low}}$ , as already observed for a fuel temperature of 1000°C (see Fig. VII-2),  $g$  does not reach such a temporary saturation level but rather approaches asymptotically the line  $Bt$  (line 1 in Fig. VII-7).

The concentration of gas in intragranular bubbles,  $b$  : the typical bell-shaped curves (Fig. VII-10) are obtained for all parameters except for  $D_{\text{low}}$ . Since bubbles are ex-

perimentally observed at a fuel temperature of 1500°C and quite low burn-up, we may conclude, that the value of  $D_{low}$  cannot be representative for in-pile conditions.

The precipitation of gas into bubbles (values of  $t$  between some minutes and several days in Fig. VII-10) is seen to depend on the bubble density,  $n$ , but not on the value of the resolution probability,  $\eta$ . In contrast, the saturation level of  $b$  (right part of the bell-shaped curves in Fig. VII-10) depends strongly on  $\eta$  and not very much on  $n$ .

Fig. VII-11 shows the influences of variations of  $D$  and  $\eta$  in more detail. The curves for  $D_{norm}$  ( $\eta$  and  $\eta/10$ ) are taken from Fig. VII-10 for comparison. If  $D$  is decreased to  $D_{med}$  (see Table VI-1), the bell-shaped curve is shifted to higher values of  $t$  without appreciable change in shape, though the curve does not reach the 100 % level. An increase in  $\eta$  leads to a lowering of the maximum and to a decreased rate of precipitation.

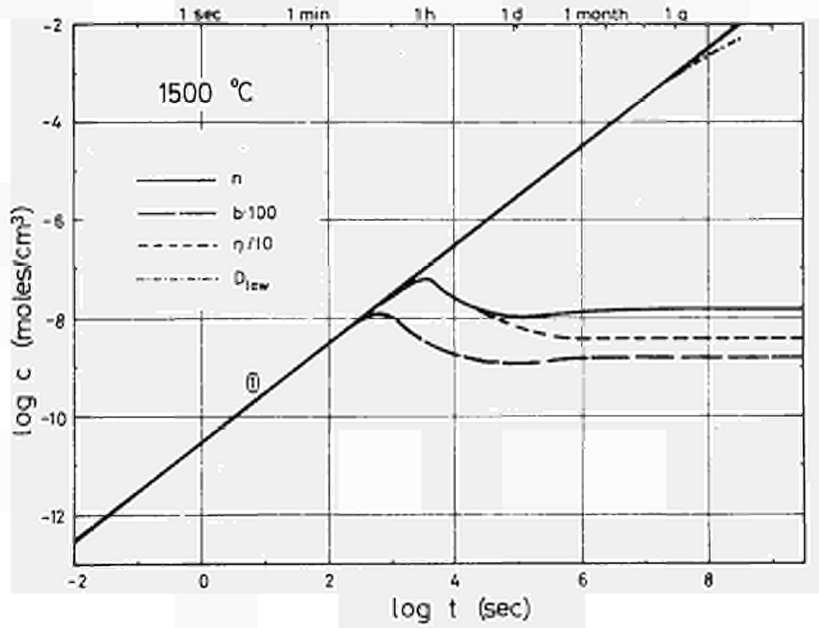


Fig. VII-6 Fission gas concentration in dynamical solution,  $c$ , for a fuel temperature of 1500°C.  $D, n$ , and  $\eta$  are varied (see Table VII-1) Line 1 represents the production of gas by fission.

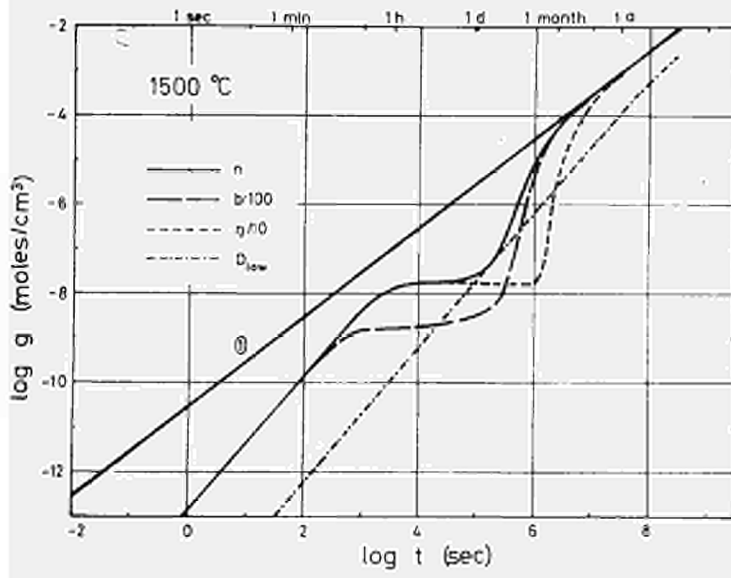


Fig. VII-7 Concentration of fission gas precipitated at grain boundaries,  $g$ , for a fuel temperature of 1500°C.  $D, n$ , and  $\eta$  are varied (see Table VII-1). Line 1 represents the production of gas by fission.

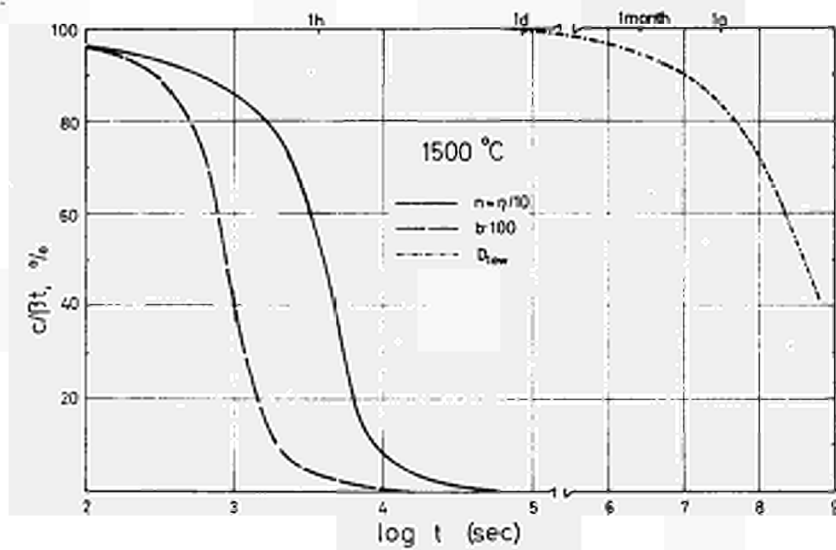


Fig. VII-8 Percentage of fission gas in dynamical solution for a fuel temperature of  $1500^{\circ}\text{C}$ .  $D, n$ , and  $\eta$  are varied (see Table VII-1)

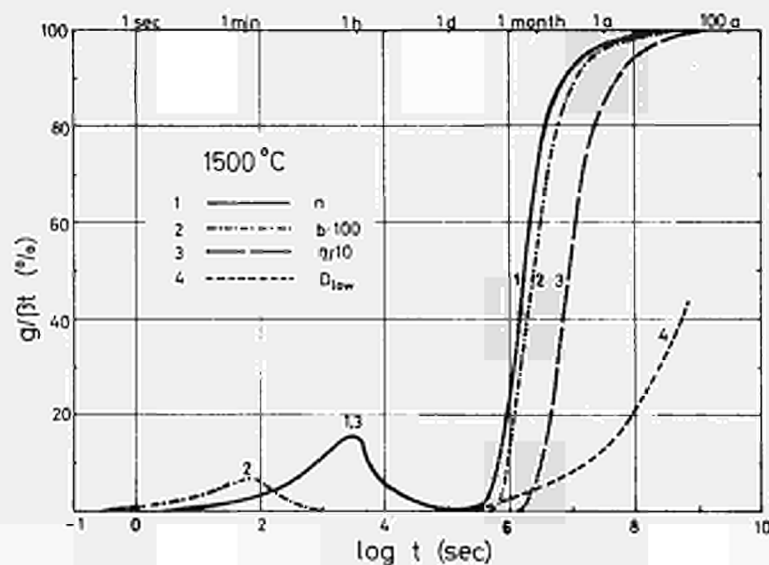


Fig. VII-9 Percentage of fission gas precipitated at grain boundaries for a fuel temperature of  $1500^{\circ}\text{C}$ .  $D, n$ , and  $\eta$  are varied (see Table VII-1)

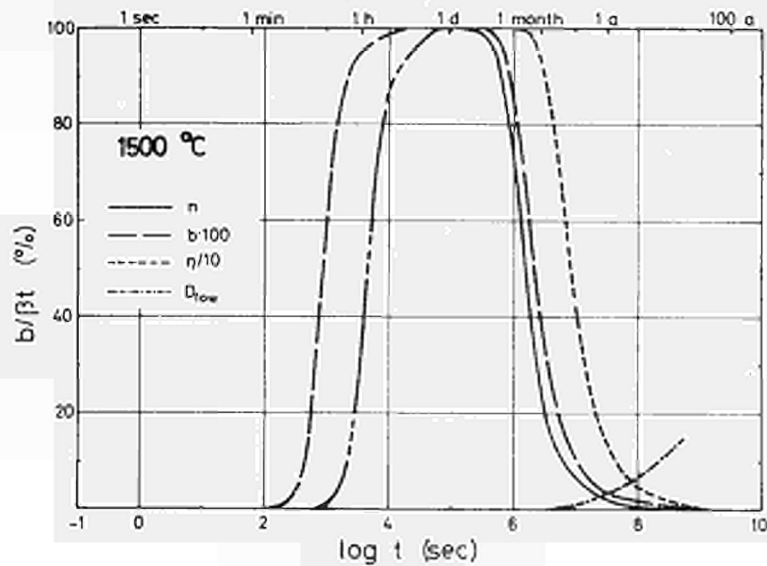


Fig. VII-10 Percentage of fission gas precipitated in intragranular bubbles for a fuel temperature of 1500°C.  $D$ ,  $n$ , and  $\eta$  are varied (see Table VII-1)

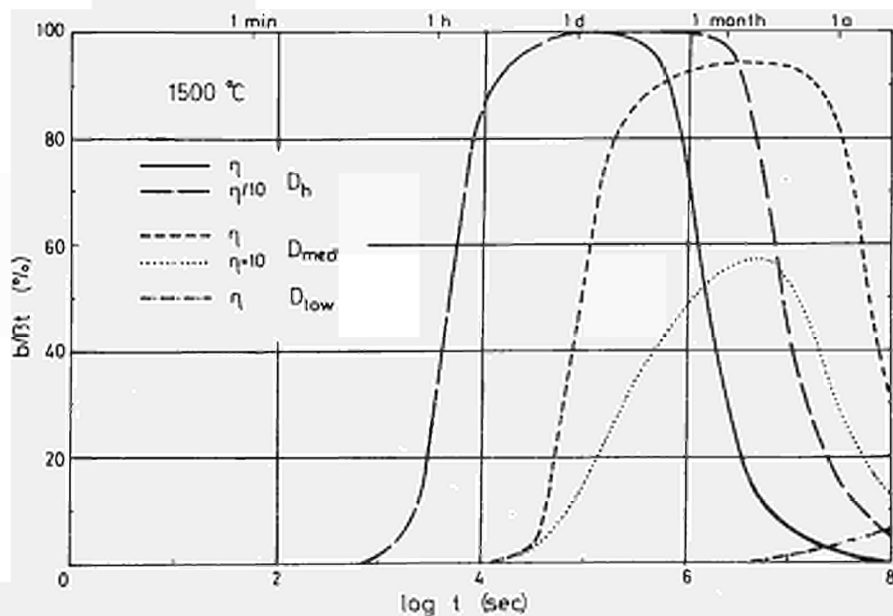


Fig. VII-11 Percentage of fission gas precipitated in intragranular bubbles for a fuel temperature of 1500°C. Three values of  $D$  are used (see Tables VI-1 and VII-1) and  $\eta$  is increased or decreased by a factor of 10.

c) Fuel temperature of 2500°C

The time dependence of  $c$ ,  $g$ , and  $b$  for a fuel temperature of 2500°C and a variation of  $D$ ,  $n$ , and  $\eta$  is shown in Figs. VII-12 to 16.

The concentration of gas in dynamical solution,  $c$ , is always very low, even for a low  $D$ -value.

The concentration of gas precipitated at grain boundaries,  $g$  is even less affected by the value of the bubble density than it is at 1500°C (see above). A reduction of the re-solution probability,  $\eta$ , by a factor of 10 again shifts the curve towards values of  $t$  which are higher by about a factor of 10 as well. Even for  $D_{low}$ ,  $g$  increases rapidly to high values indicating an important release.

The concentration of gas in intragranular bubbles,  $b$ , shows a similar behavior. The differences in the precipitation rate (left side of the bell-shaped curves in Fig. VII-16) are of mathematical interest only, since independently of the parameters used (even for  $D_{low}$ ), practically all gas is precipitated in bubbles following a few hours irradiation. The right part of the curves shows that  $b$  is affected mainly by the values of  $\eta$  and  $D$ , but that the differences are not drastic at irradiation times at which the gas content of the fuel is high. This implies small swelling rates at high fuel temperatures.

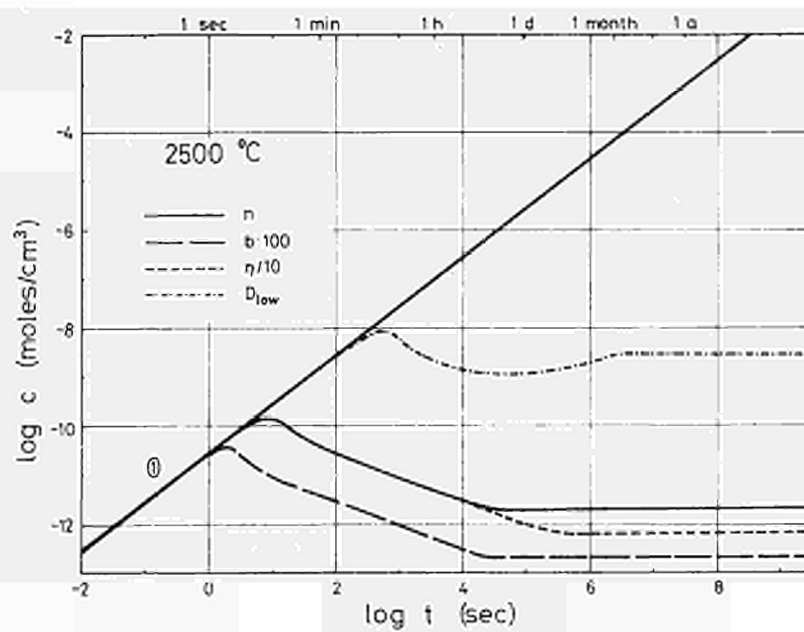


Fig. VII-12 Fission gas concentration in dynamical solution,  $c$ , for a fuel temperature of  $2500^{\circ}\text{C}$ .  $D$ ,  $n$ , and  $\eta$  are varied (see Table VII-1). Line 1 represents the production of rare gas by fission.

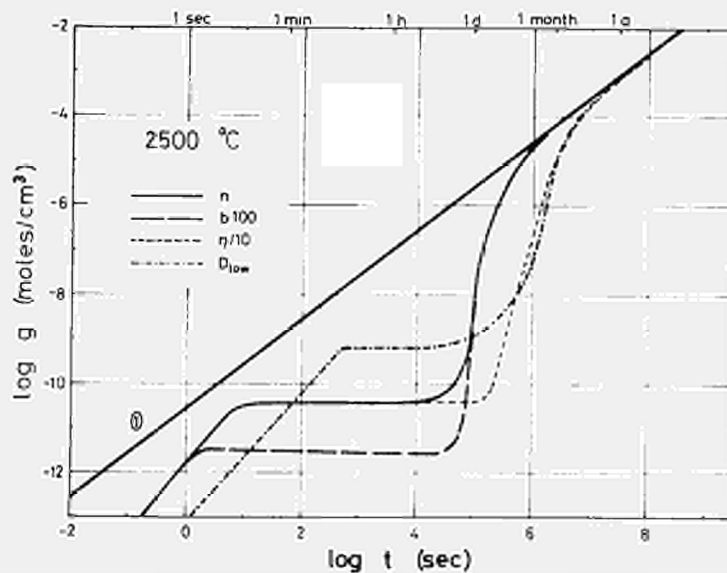


Fig. VII-13 Fission gas precipitated at grain boundaries,  $g$ , for a fuel temperature of  $2500^{\circ}\text{C}$ .  $D$ ,  $n$ , and  $\eta$  are varied (see Table VII-1). Line 1 represents the production of rare gas by fission.

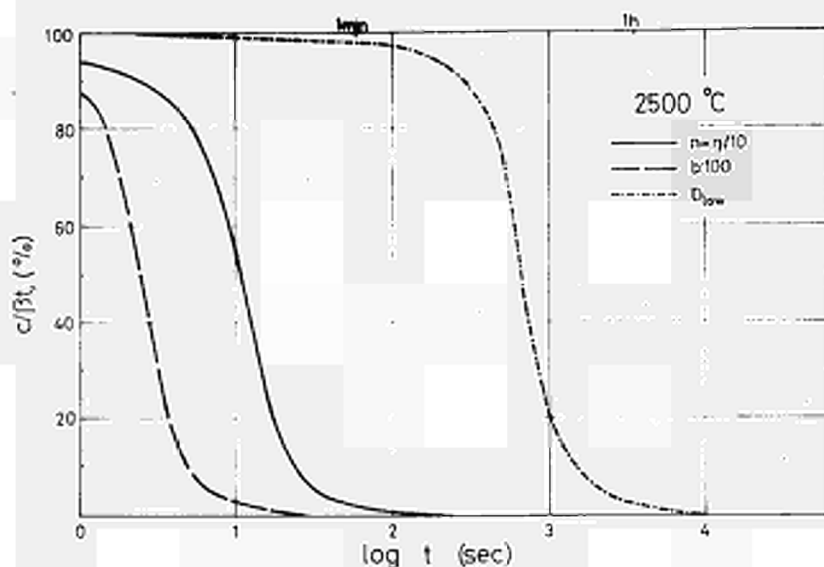


Fig. VII-14 Percentage of fission gas in dynamical solution for a fuel temperature of  $2500^\circ\text{C}$ .  $D$ ,  $n$ , and  $\eta$  are varied.

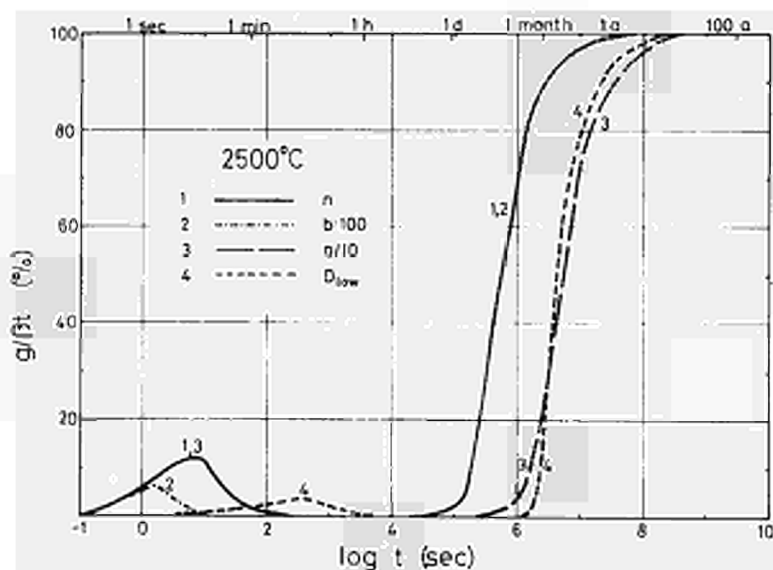


Fig. VII-15 Percentage of fission gas precipitated at grain boundaries for a fuel temperature of  $2500^\circ\text{C}$ .  $D$ ,  $n$ , and  $\eta$  are varied.

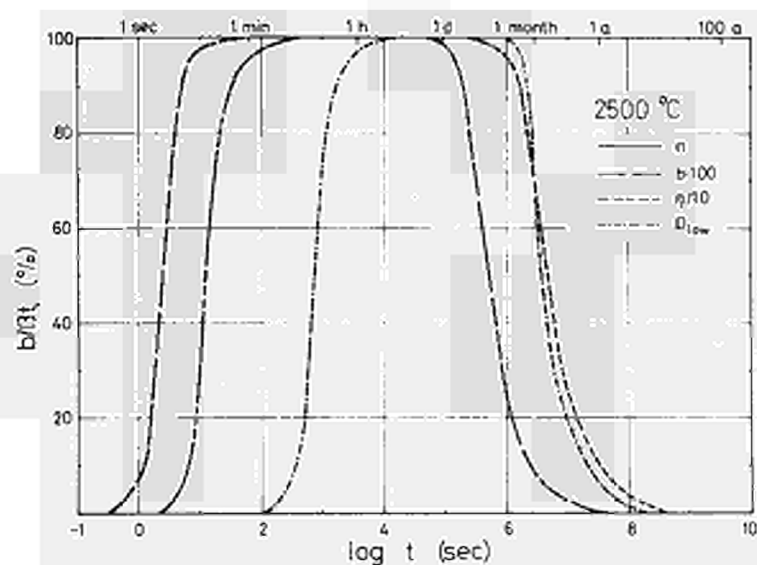


Fig. VII-16 Percentage of fission gas precipitated in intragranular bubbles for a fuel temperature of  $2500^\circ\text{C}$ .  $D$ ,  $n$ , and  $\eta$  are varied.

Appendix VIII : Variation of the re-resolution probability at  
a fuel temperature of 1200°C

The calculations for a fuel temperature of 1200°C and a variation of  $\eta$  between the "normal" value (see Table VI-1) of  $1.9 \times 10^{-5} \text{ sec}^{-1}$  and decreased to 0 in 4 steps with a factor of 10 each is shown in Figs. VIII-1 to 5.

Fig. VIII-1 shows that with decreased  $\eta$  the saturation level for high values of  $t$  decreases as well. With  $\eta = 0$ , saturation is not achieved even at unrealistically high values of  $t$ , but rather  $c$  decreases approximately with  $t^{-1/2}$ . Fig. VII-3 shows that the practical interest of this behavior is limited, especially at high burn-up.

In contrast, the dependences of  $g$  and  $b$  on  $\eta$  are of important practical interest for this medium fuel temperature where the kinetic processes are slow compared to the creation rate of gas. Fig. VIII-4 shows that only for the two highest values of  $\eta$  and for realistic irradiation times any important release can be expected. For low and medium burn-up,  $g$  is small for all values of  $\eta$ .

Similarly, any loss of gas from bubbles within realistic values of  $t$  will only be expected for the three highest values of  $\eta$  (Fig. VIII-5). For high burn-up,  $b$  and hence the swelling can vary by about a factor of 5 if  $\eta$  is reduced by a factor of 10.

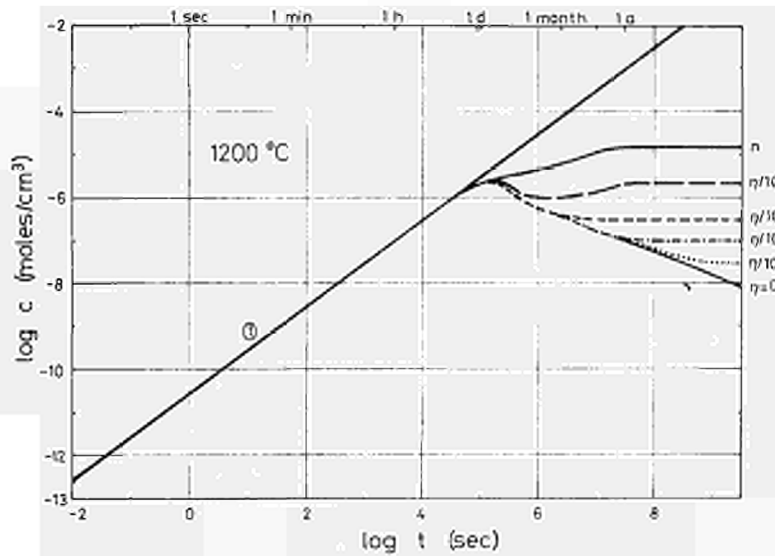


Fig. VIII-1 Concentration of gas in dynamical solution,  $c$ , for a fuel temperature of 1200°C and a variation of  $\eta$ . Line 1 represents the production of rare gas by fission.

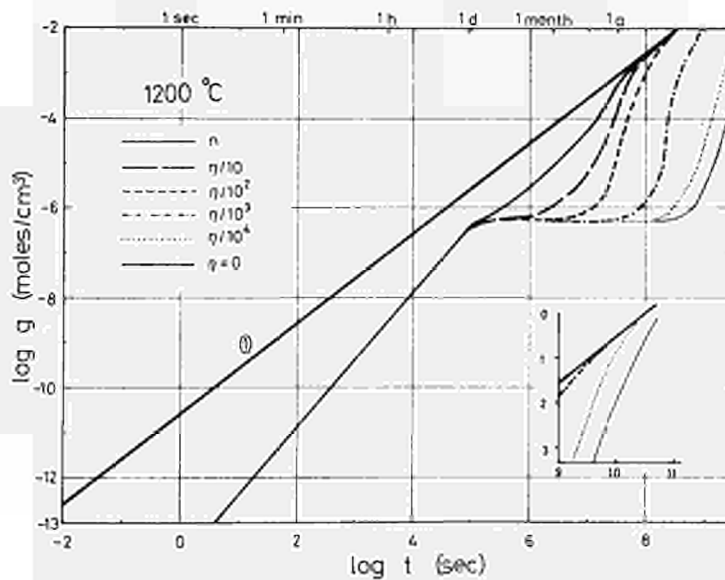


Fig. VIII-2 Concentration of gas precipitated at grain boundaries,  $g$ , for a fuel temperature of 1200°C and a variation of  $\eta$ . Line 1 represents the production of rare gas by fission.

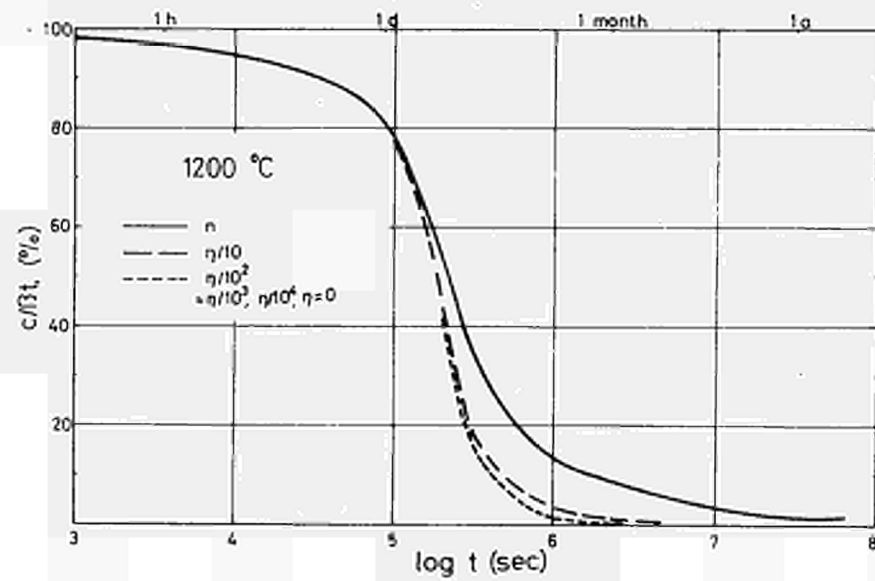


Fig. VIII-3 Percentage of fission gas in dynamical solution for a fuel temperature of  $1200^{\circ}\text{C}$  and a variation of  $\eta$ .

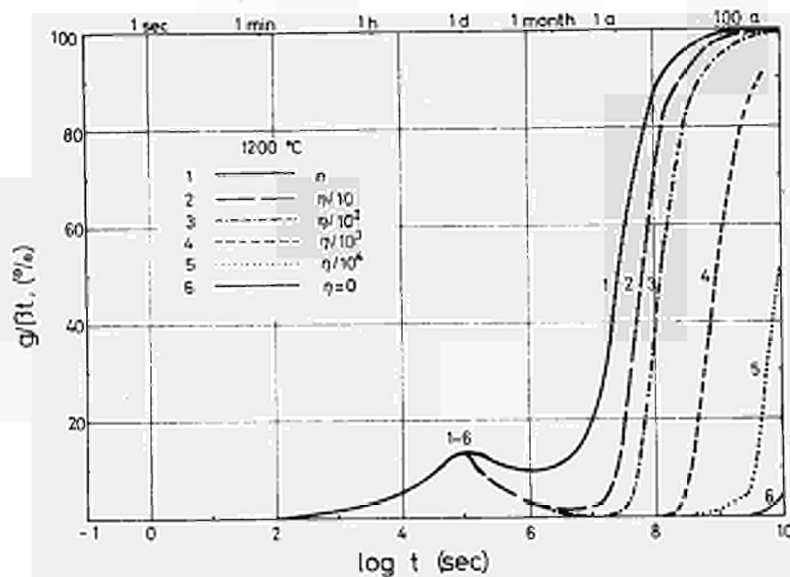


Fig. VIII-4 Percentage of fission gas precipitated at grain boundaries for a fuel temperature of  $1200^{\circ}\text{C}$  and a variation of  $\eta$ .

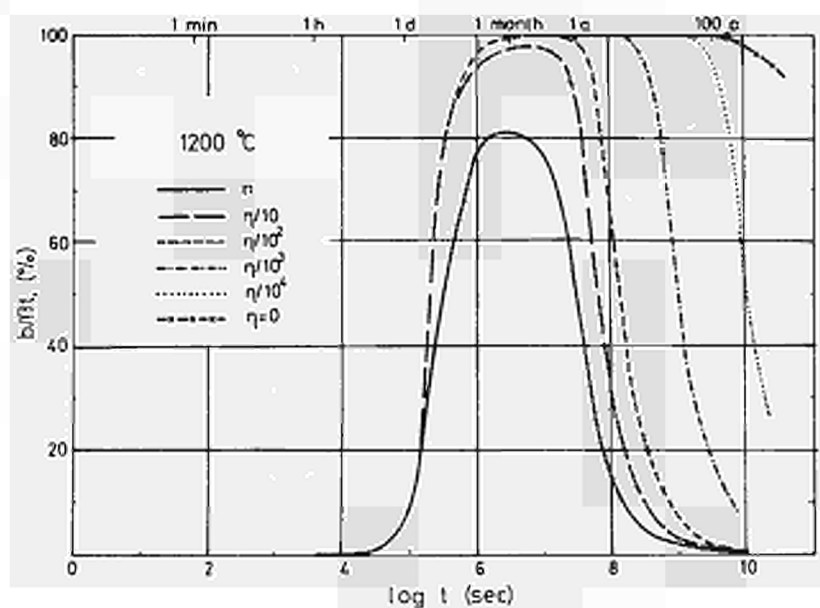


Fig. VIII-5 Percentage of fission gas precipitated in intragranular bubbles for a fuel temperature of  $1200^{\circ}\text{C}$  and a variation of  $\eta$ .

Appendix IX : Variation of the gas diffusion coefficient, D, and the grain size, a, at a fuel temperature of 2000°C.

The calculations for a grain size of 10  $\mu\text{m}$  are shown in Figs. IX-1 to 5. The gas diffusion coefficient is varied in four steps between  $10^{-9}$  and  $10^{-12}$   $\text{cm}^2\text{sec}^{-1}$ . This region corresponds to the combined scatter of Stage II A (free gas diffusion) and Stage II B (trapping) at 2000°C (see Fig. III-2).

The concentration of gas in dynamical solution, c, is shown in Figs. IX-1 and 3. The equilibrium value is reached very fast (within  $\approx 1\text{d}$ ) and is roughly inversely proportional to D.

The percentage of gas at grain boundaries, g, (see Figs. IX-2 and 4) shows pronounced maxima at small values of t which increase with increasing diffusion coefficients. Again, these maxima are unimportant for practice due to the small gas concentration at these small values of t. The subsequent transport of gas to the grain boundaries depends very little on D. Both phenomena are due to the fact that the kinetics are very fast as compared to the chosen small grain size (see also the different behavior for  $a = 100 \mu\text{m}$  shown below).

The concentration of gas in intragranular bubbles, b, (see Fig. IX-5) shows a similar behavior, i.e. a strong dependence on D is only observed for short times (rate of precipitation), whereas the behavior after having attained saturation is identical for the three higher values of D, as already observed for g (see Fig. IX-4). This again is due to the fast mobility and the small grain size which leads to a sudden transition from the state of predominant precipitation to a predominant migration to the grain boundaries (see Fig. IX-2). Such an effect is not observed for bigger grain sizes (see below).

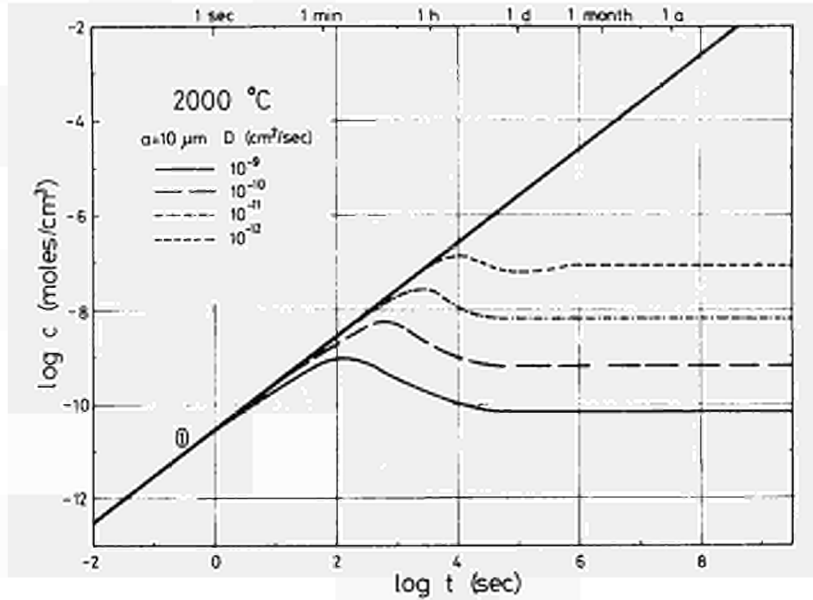


Fig. IX-1 Concentration of gas in dynamical solution,  $c$ , for a fuel temperature of  $2000^\circ\text{C}$  and a variation of  $D$ . The grain size  $a$  is  $10 \mu\text{m}$ . Line 1 represents the production of the gas by fission.

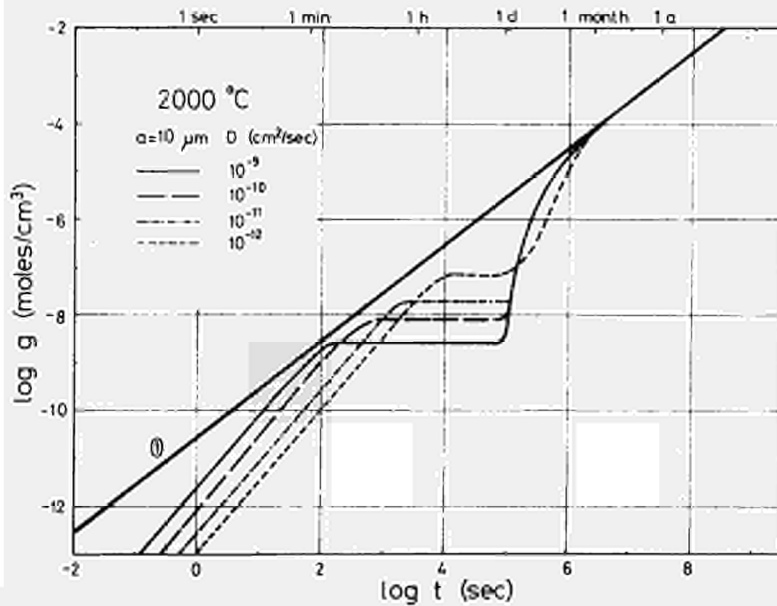


Fig. IX-2 Concentration of gas precipitated at the grain boundaries,  $g$ , for a fuel temperature of  $2000^\circ\text{C}$  and a variation of  $D$ . The grain size  $a$  is  $10 \mu\text{m}$ . Line 1 represents the production of the gas by fission.

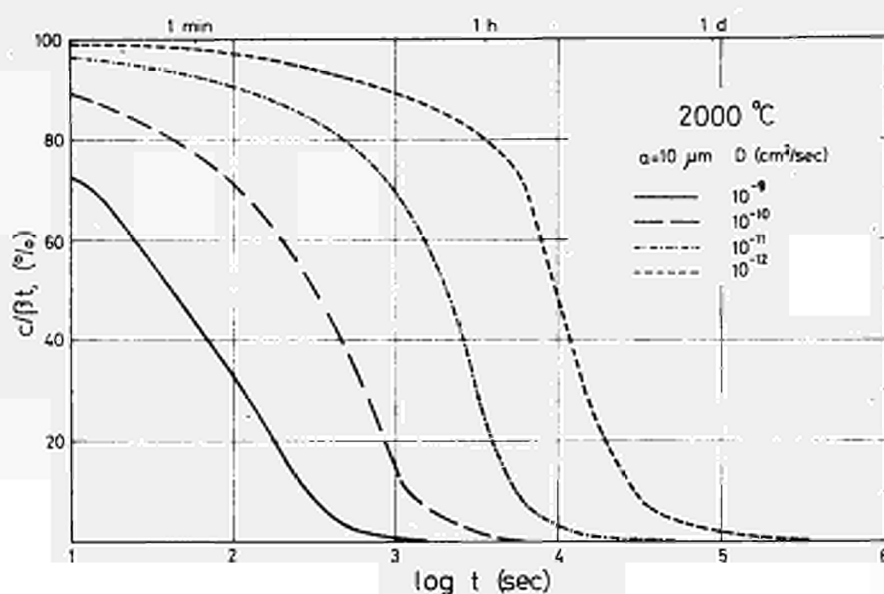


Fig. IX-3 Percentage of the gas in dynamical solution for a fuel temperature of 2000°C and a variation of D. The grain size is 10 μm.

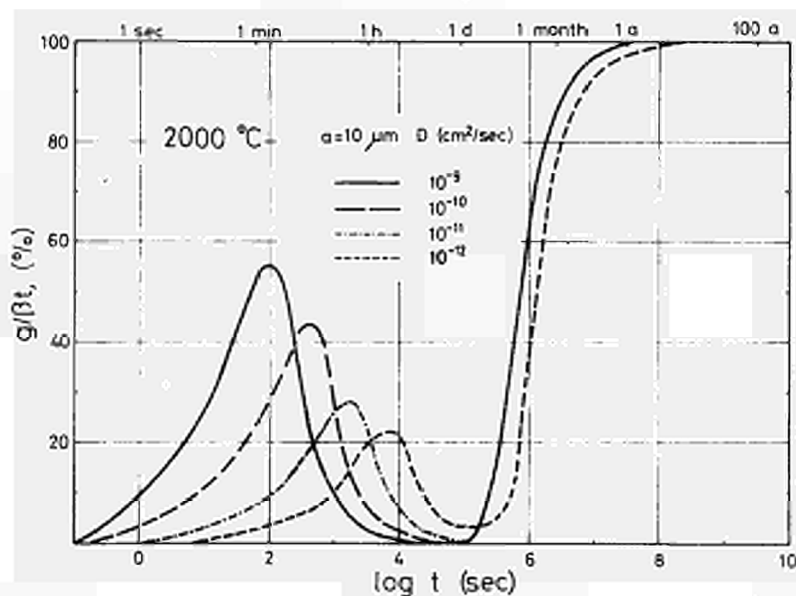


Fig. IX-4 Percentage of the gas precipitated at grain boundaries for a fuel temperature of 2000°C and a variation of D. The grain size is 10 μm.

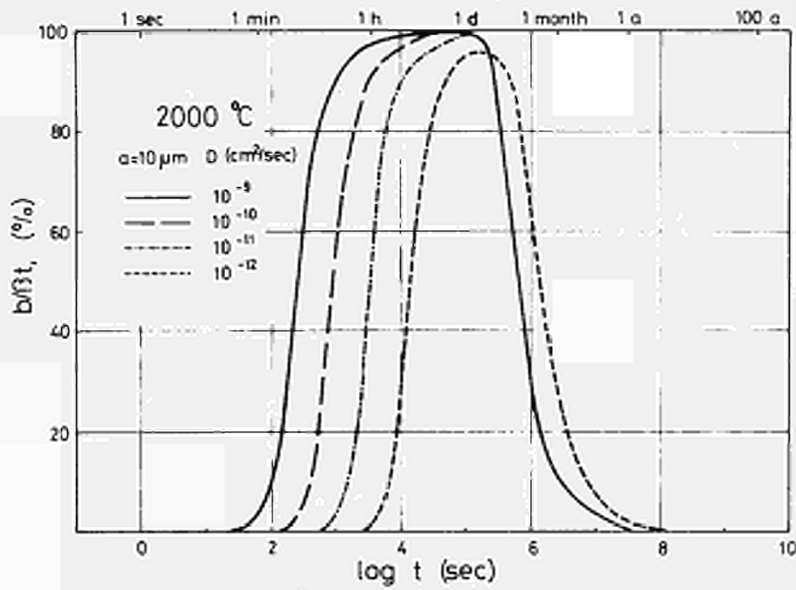


Fig. IX-5 Percentage of gas precipitated in intragranular bubbles for a fuel temperature of  $2000^\circ\text{C}$  and a variation of  $D$ . The grain size is  $10\ \mu\text{m}$ .

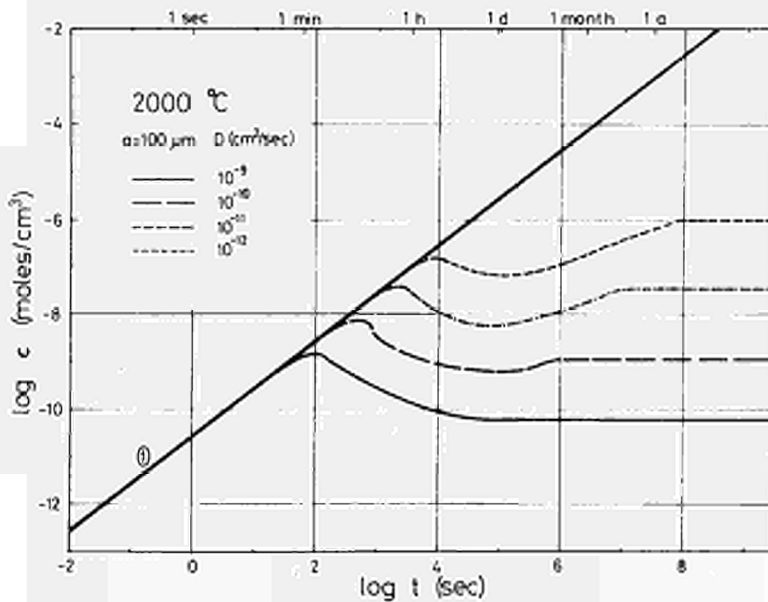


Fig. IX-6 Concentration of gas in dynamical solution,  $c$ , for a fuel temperature of  $2000^\circ\text{C}$  and a variation of  $D$ . The grain size  $a$  is  $100\ \mu\text{m}$ . Line 1 represents the production of the gas by fission.

The results for a grain size of 100  $\mu\text{m}$  and the same four values of D are shown in Figs. IX-6 to 10. In contrast to the results for  $a = 10 \mu\text{m}$ , differences are observed for c, g, and b for the different D-values. Basically, the curves showing the percentage of c, g, and b (Figs. IX-8 to 10) are shifted towards higher values of t if D is decreased thus reflecting the decrease in kinetic rates. This behavior is typical for conditions in which none of the competing processes of creation, precipitation, resolution and migration to the grain boundaries dominates the remaining ones.

In the remaining figs. IX-11 to 13, the effect of varying the grain size for a given value of D ( $= 10^{-10} \text{ cm}^2 \text{ sec}^{-1}$ ) is shown. Obviously, the percentage of c does not change appreciably with a variation of a. In contrast, both g and b show the expected retarded release and a corresponding increase of swelling if a is increased. One should note that the details of the trend presented in Figs. IX-12 and 13 are representative only for the particular temperature and D-value used.

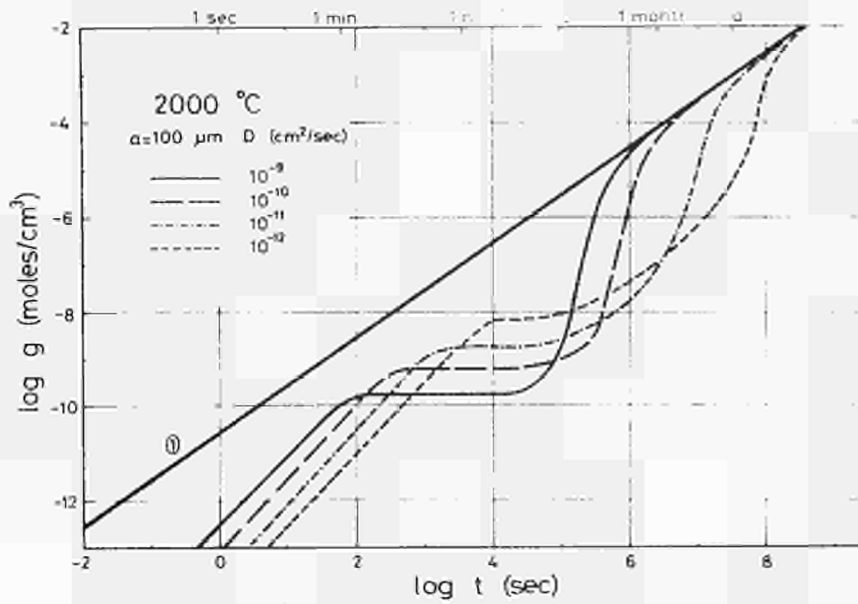


Fig. IX-7 Concentration of gas precipitated at the grain boundaries,  $g$ , for a fuel temperature of 2000°C and a variation of  $D$ . The grain size  $a$  is 100  $\mu\text{m}$ . Line 1 represents the production of the gas by fission.

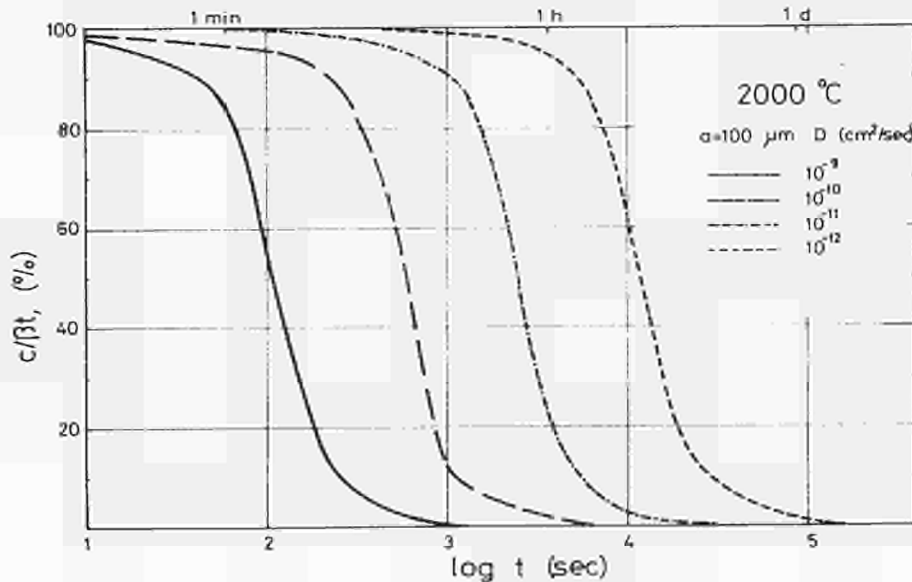


Fig. IX-8 Percentage of the gas in dynamical solution for a fuel temperature of 2000°C and a variation of  $D$ . The grain size is 100  $\mu\text{m}$ .

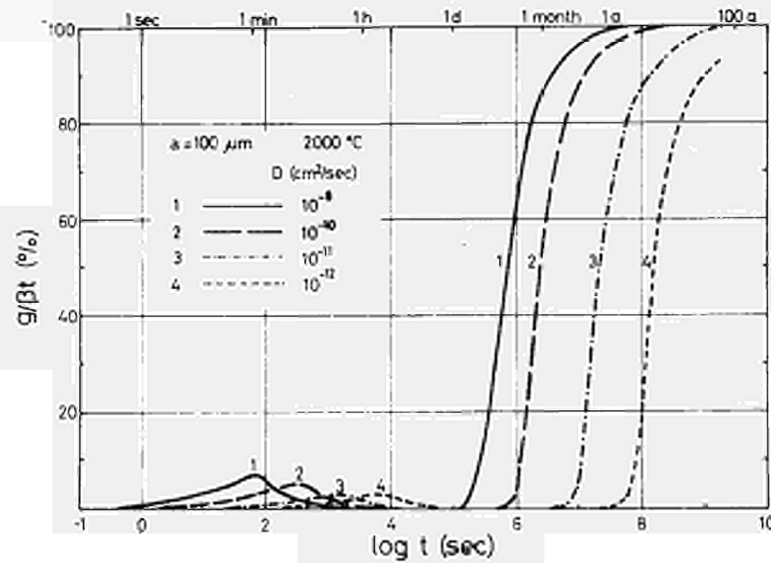


Fig. IX-9 Percentage of the gas precipitated at grain boundaries for a fuel temperature of 2000°C and a variation of D. The grain size is 100 μm.

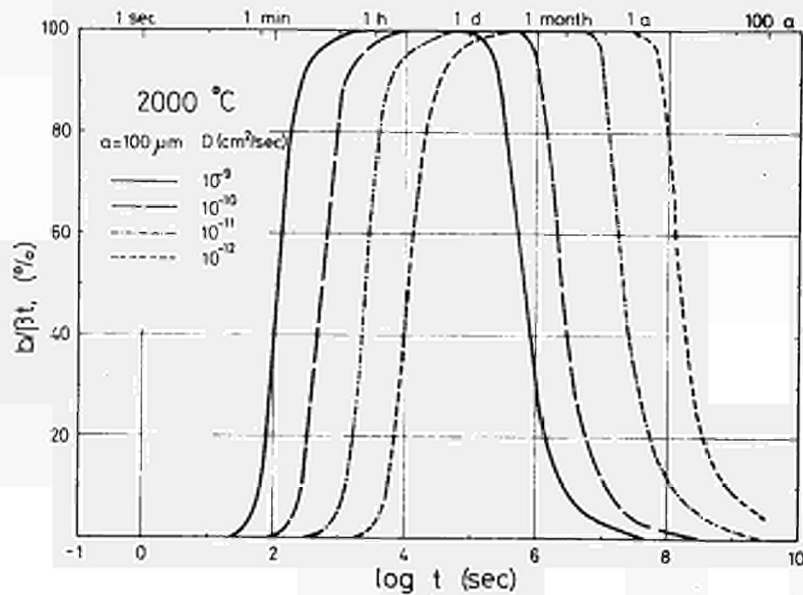


Fig. IX-10 Percentage of gas precipitated in intragranular bubbles for a fuel temperature of 2000°C and a variation of D. The grain size is 100 μm.

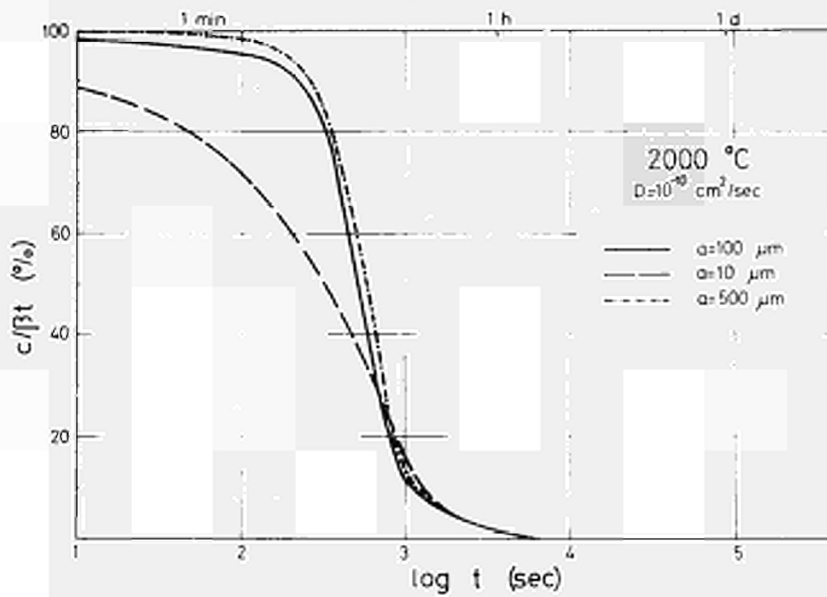


Fig. IX-11 Percentage of the gas in dynamical solution for a fuel temperature of  $2000^\circ\text{C}$  and a D-value of  $10^{-10} \text{ cm}^2 \text{ sec}^{-1}$ . The grain size is varied (10, 100, 500  $\mu\text{m}$ ).

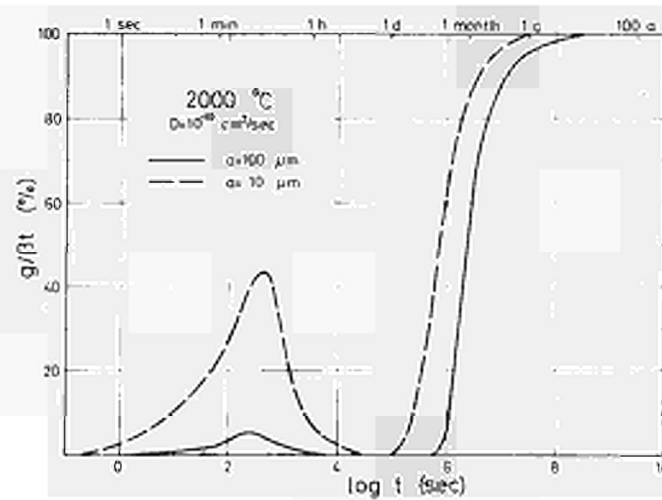


Fig. IX-12 Percentage of the gas precipitated at grain boundaries for a fuel temperature of  $2000^\circ\text{C}$  and a D-value of  $10^{-10} \text{ cm}^2 \text{ sec}^{-1}$ . The grain size is varied (10, 100  $\mu\text{m}$ ).

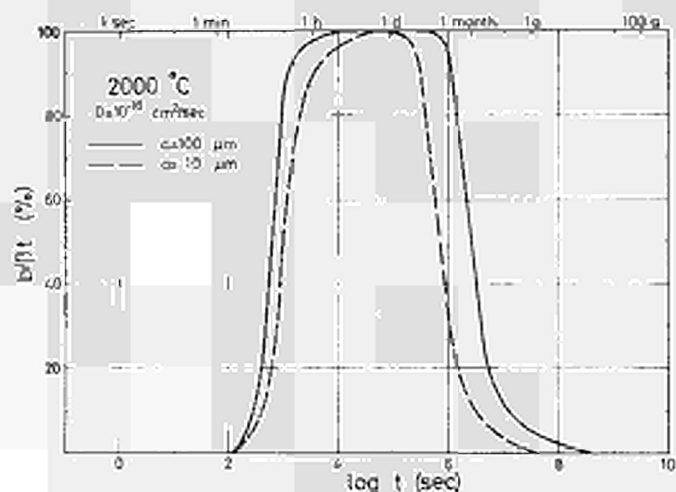
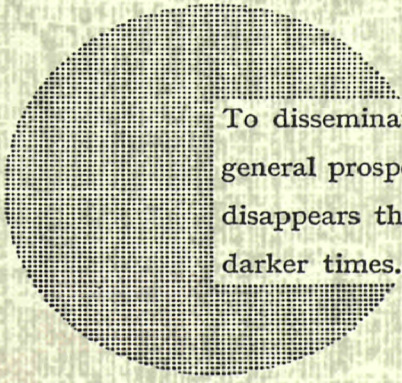


Fig. IX-13 Percentage of gas precipitated in intragranular bubbles for a fuel temperature of 2000°C and a D-value of  $10^{-10}$  cm<sup>2</sup> sec<sup>-1</sup>. The grain size is varied (10, 100 μm).

## NOTICE TO THE READER

All scientific and technical reports published by the Commission of the European Communities are announced in the monthly periodical "**euro-abstracts**". For subscription (1 year: B.Fr. 1 025,—) or free specimen copies please write to:

Office for Official Publications  
of the European Communities  
Case postale 1003  
Luxembourg 1  
(Grand-Duchy of Luxembourg)



To disseminate knowledge is to disseminate prosperity — I mean general prosperity and not individual riches — and with prosperity disappears the greater part of the evil which is our heritage from darker times.

Alfred Nobel

## SALES OFFICES

The Office for Official Publications sells all documents published by the Commission of the European Communities at the addresses listed below, at the price given on cover. When ordering, specify clearly the exact reference and the title of the document.

### GREAT BRITAIN AND THE COMMONWEALTH

*H.M. Stationery Office*  
P.O. Box 569  
London S.E. 1

### UNITED STATES OF AMERICA

*European Community Information Service*  
2100 M Street, N.W.  
Suite 707  
Washington, D.C. 20 037

### BELGIUM

*Moniteur belge — Belgisch Staatsblad*  
Rue de Louvain 40-42 — Leuvenseweg 40-42  
1000 Bruxelles — 1000 Brussel — Tel. 12 00 26  
CCP 50-80 — Postgiro 50-80

*Agency :*  
Librairie européenne — Europese Boekhandel  
Rue de la Loi 244 — Wetstraat 244  
1040 Bruxelles — 1040 Brussel

### GRAND DUCHY OF LUXEMBOURG

*Office for official publications  
of the European Communities*  
Case postale 1003 — Luxembourg 1  
and 29, rue Aldringen, Library  
Tel. 4 79 41 — CCP 191-90  
Compte courant bancaire : BIL 8-109/6003/200

### FRANCE

*Service de vente en France des publications  
des Communautés européennes*  
26, rue Desaix  
75 Paris-15<sup>e</sup> — Tel. (1) 306.5100  
CCP Paris 23-96

### GERMANY (FR)

*Verlag Bundesanzeiger*  
5 Köln 1 — Postfach 108 006  
Tel. (0221) 21 03 48  
Telex : Anzeiger Bonn 08 882 595  
Postscheckkonto 834 00 Köln

### ITALY

*Libreria dello Stato*  
Piazza G. Verdi 10  
00198 Roma — Tel. (6) 85 09  
CCP 1/2640

*Agencies :*  
00187 Roma — Via del Tritone 61/A e 61/B  
00187 Roma — Via XX Settembre (Palazzo  
Ministero delle finanze)  
20121 Milano — Galleria Vittorio Emanuele 3  
80121 Napoli — Via Chiaia 5  
50129 Firenze — Via Cavour 46/R  
16121 Genova — Via XII Ottobre 172  
40125 Bologna — Strada Maggiore 23/A

### NETHERLANDS

*Staatsdrukkerij- en uitgeverijbedrijf*  
Christoffel Plantijnstraat  
's-Gravenhage — Tel. (070) 81 45 11  
Giro 425 300

### IRELAND

*Stationery Office*  
Beggars Bush  
Dublin 4

### SWITZERLAND

*Librairie Payot*  
6, rue Grenus  
1211 Genève  
CCP 12-236 Genève

### SWEDEN

*Librairie C.E. Fritze*  
2, Fredsgatan  
Stockholm 16  
Post Giro 193, Bank Giro 73/4015

### SPAIN

*Librería Mundi-Prensa*  
Castello, 37  
Madrid 1

### OTHER COUNTRIES

*Sales Office for official publications  
of the European Communities*  
Case postale 1003 — Luxembourg 1  
Tel. 4 79 41 — CCP 191-90  
Compte courant bancaire : BIL 8-109/6003/200